Tectonophysics 787 (2020) 228471

Contents lists available at ScienceDirect

Tectonophysics

journal homepage: www.elsevier.com/locate/tecto

The Kefalonia Transform Fault: A STEP fault in the making

Ali Değer Özbakır[a,*], Rob Govers[a], Andreas Fichtner[b]

[a] Department of Earth Sciences, Tectonophysics group, Universiteit Utrecht, Utrecht, the Netherlands
[b] Department of Earth Sciences, ETH Zürich, Zürich, Switzerland

ARTICLE INFO

Keywords:
Subduction zone processes
Tomography
STEPs
Slab segmentation
Hellenic Subduction Zone

ABSTRACT

Vertical edges along subducted slabs have been recognized in the majority of subduction zones. Surprisingly, slab edges evolved into Subduction-Transform-Edge-Propagator (STEP) faults in only a few regions; the conditions under which STEPs form are special. It is relevant to constrain the conditions that facilitate STEP fault initiation because they leave a clear geological footprint in the overriding plate, whereas vertical tears generally do not. We therefore study a candidate region for STEP fault initiation in the western Hellenic Subduction Zone.

We investigate the structure and seismicity of the shallow western Hellenic Subduction Zone using a recent full-waveform inversion model which both captures details of crustal and upper-mantle structure, yielding constraints in the depth interval from 10 to 200 km where lithosphere-mantle interactions have tectonic expressions. The western end of the Hellenic Subduction Zone is fragmented near the Kefalonia Transform Fault. We identify a separate Epirus lithospheric fragment that is roughly vertical below the southern Albanides. We also identify a new and major contrast within the lithospheric mantle of the Ionian ocean basin, which aligns with a gradient in free-air anomalies.

In the overriding plate, the Kefalonia Transform Fault zone accommodates right lateral strike-slip deformation. We interpret this fault zone as a proto-STEP fault that formed simultaneously with Pliocene fragmentation of the Epirus fragment.

Comparing the recent evolution of the NW Hellenic slab edge with currently active STEPs indicates that along-trench variations in convergence velocity are a prerequisite for STEP fault initiation. Such velocity variations may result from subduction of continental crust along part of the trench. Resistance to sea ward tear propagation by a mechanically strong subducting plate may prevent variations in convergence velocity to occur, and thus STEP fault initiation. The amount of time over which a velocity contrast persists will also be relevant for STEP fault initiation. Mechanical coupling between upper- and lower-plate, and the deformability of the upper-plate appear to also play a role in the initiation of the STEP fault once a slab is fragmented.

1. Introduction

Lateral edges have been recognized along or within various subducted slabs (Fig. 1; present-day, unless indicated otherwise); including Nazca slab (Gutscher et al., 1999; Pesicek et al., 2012), Izu-Bonin slab (Fryer et al., 2003; Gvirtzman and Stern, 2004; Miller et al., 2004, 2005, 2006a, 2006b; Gong et al., 2018), south Lesser Antilles slab (Russo et al., 1993; Clark et al., 2008; Van Benthem et al., 2013), various Mediterranean slabs (Spakman et al., 1988; Carminati et al., 1998; Wortel and Spakman, 2000; Biryol et al., 2011; Jolivet et al., 2013; de Lis Mancilla et al., 2018), Zagros/Makran slab (Agard et al., 2011), Pamir slab (Sippl et al., 2013; Sobel et al., 2013; Thiede et al., 2013), Burma slab (Kumar et al., 2016), Sikkim slab (Zhang et al., 2017; Sunilkumar et al., 2019), Philippine Sea slab near Taiwan (Lallemand et al., 1997), northern Scotia slab (Forsyth, 1975), eastern Sunda slab (Spakman and Hall, 2010), north Tonga slab (Isacks et al., 1969; Millen and Hamburger, 1998), Kermadec-Hikurangi slab (Reyners and Robertson, 2004), and Solomon slab (Neely and Furlong, 2018). Surprisingly, these slab edges evolved into Subduction-Transform-Edge-Propagators (STEPs; Govers and Wortel, 2005) in only very few regions, i.e., the conditions under which STEPs form require other conditions in addition to slab fragmentation. Understanding these conditions is particularly relevant because a slab edge seldom leaves a clear tectonic imprint in the crust of the overriding plate. This is different for STEP faults sensu Baes et al. (2011); their footprint in the tectonic evolution of basins (such as vertical axis rotations, topography build-up, fast trench roll-back) attests to the relevance of STEP activity (e.g., Mediterranean subduction zones, Tonga trench, South Sandwich trench,

* Corresponding author.
E-mail address: aozbakir@gmail.com (A.D. Özbakır).

https://doi.org/10.1016/j.tecto.2020.228471
Received 13 January 2020; Received in revised form 27 April 2020; Accepted 4 May 2020
Available online 17 May 2020

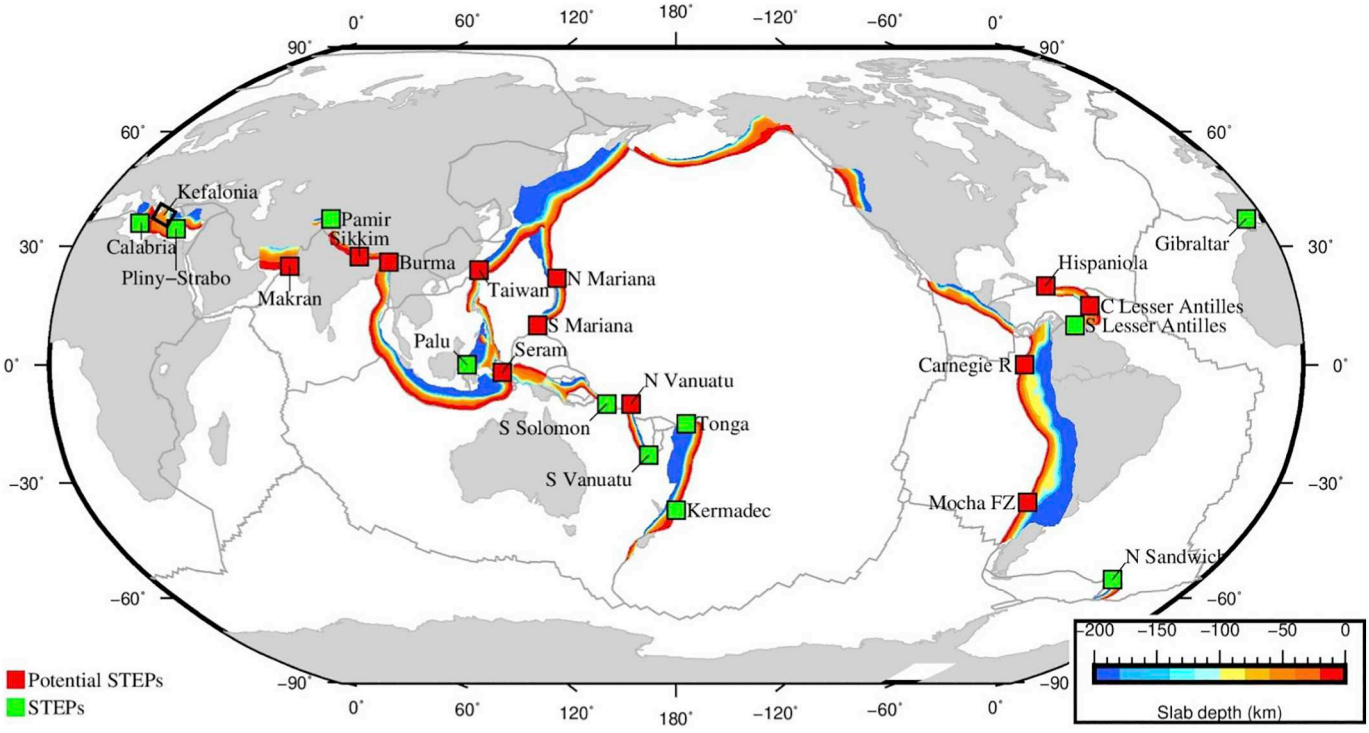

Fig. 1. Global overview of slabs with a vertical tear or a lateral edge that are associated with a STEP fault in the overriding plate ("STEPs"), or not ("Potential STEPs"). Slab depth contours (Hayes et al., 2018) are shown in colors, along with plate boundaries from (Bird, 2003).

southern edge of the Lesser Antilles trench, and the western edge of north Sulawesi trench; Govers and Wortel (2005)). We therefore seek to constrain the conditions that facilitate STEP fault initiation in a region where slab edge creation by fragmentation may have recently started. Govers and Wortel (2005) suggested that the offshore Kefalonia Transform Fault (KTF; Fig. 2) and its on-land continuation constitute a STEP fault. Available geological constraints, discussed below, suggest that the system would be in an infant stage. We study this candidate region for STEP fault initiation in the western Hellenic Subduction Zone.

Here, the active deformation pattern of the overriding Eurasian lithosphere is complex, and its interpretation in terms of the driving forces non-unique. Likely contributors are rollback of the Hellenic slab and backarc extension, westward motion of Anatolia facilitated by the North Anatolian Fault/North Aegean Trough, strain localization in the Gulf of Corinth (GC) collision in the Dinarides/Albanides, Nubia convergence, mantle convective tractions including dynamic topography, gravitational collapse, and potentially STEP fault activity (Jolivet et al., 2013). We do not aim to quantify their relative contributions to the deformation of the overriding plate. Rather, our focus is primarily on the structure of the Hellenic slab near the KTF. The reason is that the interpretation of the deformation of the overriding plate in terms of a STEP fault hinges on the lateral continuity of the slab. We discuss recent studies of the lateral continuity of the shallow (50–200 km depth) slab and conclude that none of these were conclusive. We present and interpret the results of the regional shear wave velocity tomographic volume of Fichtner et al. (2013). As it is based on a tomographic imaging technique that employs complete seismograms from regional broadband stations, this model captures relevant details in both the crustal and upper-mantle structure between 10 and 200 km depth, where lithosphere–mantle interactions forge tectonic expressions.

The regional context of our study area is slow Africa-Eurasia convergence and ongoing closure of the Mediterranean land-locked basin (Le Pichon, 1982). Some of mostly ephemeral plate boundary segments undergo soft collision (Royden, 1993), while adjacent segments accommodate oceanic subduction with a significant component of trench retreat. Slab roll-back and backarc extension occur at relatively fast rates, and these processes have had a large imprint on the evolution of the Mediterranean region during the last 20 Ma (Wortel and Spakman, 2000). In the eastern Mediterranean, Mio-Pliocene shortening in the external Dinarides in response to the collision of the Adria promontory (Africa) was limited in southern Montenegro and north Albania (Bega, 2015; Van Unen et al., 2019), and moderate in central Albania (Handy et al., 2019). The northern Hellenides thrust belt also continues to shorten today. Further to the southeast along the plate boundary, the influence of rollback of the Hellenic slab leads to foreland-propagating nappes in the southern Hellenides (Underhill, 1989), where the thrust front has stepped back to the subduction boundary south of Ionian islands (Royden and Papanikolaou, 2011). The KTF represents the approximate boundary between the subduction of oceanic lithosphere to the south and continental (Adria) lithosphere to the north (Fig. 2). GNSS velocities in the overriding plate show a strong gradient near the KTF (Fig. 3). All these observations suggest that the KTF marks a lithospheric boundary.

This paper is organized as follows. In Section 2 we discuss previous studies on the structure and continuity/discontinuity of the Hellenic slab in our study area. We also outline the main results from seismicity studies. In Section 3 we present the data and methods that were used in the tomographic inversion, and for constraining the hypocenter of $M > 4$ subcrustal earthquakes. Section 4 presents the tomographic results and their interpretation. In Section 5 we review the recent and active deformation of the overriding plate. Here we conclude that a proto-STEP fault is active in the overriding plate. The Late Miocene-Pliocene geological history as recorded in the overriding plate is the topic of Section 6; here we aim to constrain the evolution of the Hellenic slab given what we learned about its structure today. This scenario for the slab fragmentation history and its corresponding imprint on the overriding plate is used in Section 7 to distill the tectonic conditions that resulted in the formation of the KTF STEP fault, and to globally compare these conditions with those of regions where STEP faults did, and did not, develop.

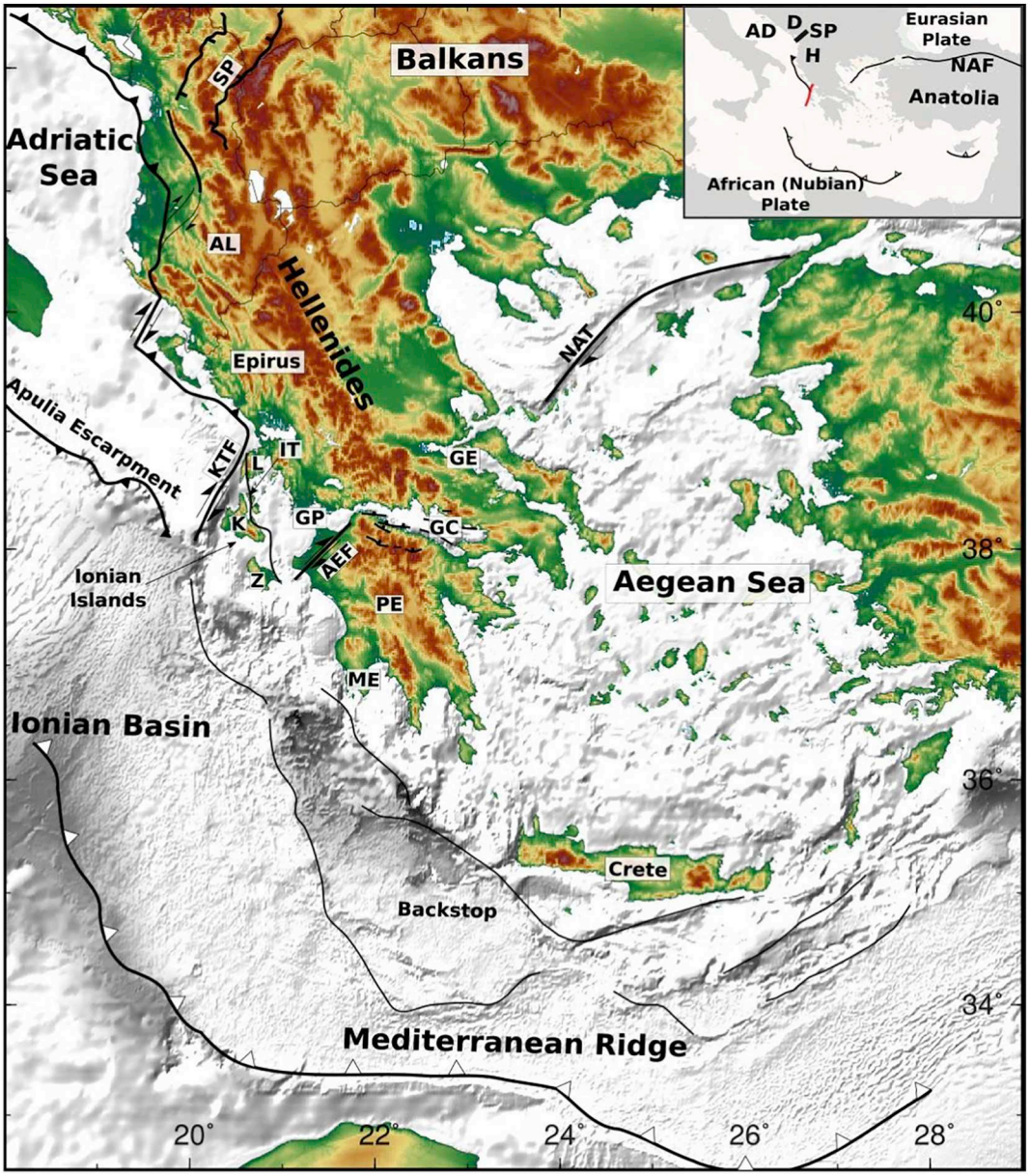

Fig. 2. Topography/bathymetry of the Hellenic subduction zone and major faults. Thick black lines represent the approximate location of plate contacts and major faults simplified from Chamot-Rooke et al. (2005) and Handy et al. (2019), and the trench physiography is shown with thin barbed black lines. Abbreviations refer to: AEF: Achaia-Elia fault; GC: Gulf of Corinth; GE: Gulf of Evia; GP: Gulf of Patras; IT: Ionian Thrust; K: Kefalonia; L: Levkas; ME: Messenia; PE: Peloponnesus; SP: Scutari-Pec; Z: Zakynthos; KTF: Kefalonia Transform Fault; NAT: North Aegean Trough; Inset map shows central and eastern Mediterranean subduction/collision zones. A: Albanides, AD: Adria, Ap: Apulia, D: Dinarides, H: Hellenides, NAF: North Anatolian Fault, SP: Scutari-Pec.

2. Summary of previous studies

2.1. Tomography studies

The velocity structure of the western Hellenic subduction zone was investigated in classical body-wave tomography studies, which outlined the Hellenic slab in the mantle (Spakman et al., 1988, 1993; Papazachos and Nolet, 1997; Bijwaard and Spakman, 2000; Piromallo and Morelli, 2003). These studies interpreted a slab that is laterally continuous from Crete to the southern Peloponnesus, and that extends downward into the lower mantle (Spakman et al., 1993; Bijwaard and Spakman, 2000; Piromallo and Morelli, 2003; Zhu et al., 2015). However, the continuity of the slab towards the northwest is unclear. In a more recent body-wave tomography study, Hansen et al. (2019) found evidence for horizontal slab detachment 150–250 km below the entire Peloponnesus. They conclude that there is no slab in this depth range to the north of the Gulf of Patras (Fig. 2). They infer a lithospheric fragment in the mantle below the Epirus region (Fig. 2). Regional scale surface-wave tomography studies showed low-velocities in the mantle north of the GC in the depth range ~ 60–200 km, which are interpreted to be thermally induced (Bourova et al., 2005; Salaün et al., 2012).

Further towards the northwest along Dinarides/Albanides plate boundary, the results of tomographic imaging are somewhat ambiguous, particularly below 150 km. The northern Dinarides are underlain by mantle velocities down to 300–400 km depth (Koulakov et al., 2009; Zhu et al., 2015; Van der Meer et al., 2018). For the southern Dinarides, the tomographic models show a high-velocity anomaly down to 200 km depth (Koulakov et al., 2009; Van der Meer et al., 2018) or to the top of the transition zone (Piromallo and Morelli, 2003; Zhu et al., 2015). The absence of high-velocity anomalies below the northern Dinarides and its southward continuation led Wortel and Spakman (1992) to propose that the slab detached here (Fig. 4A - Detachment model). The Scutari-

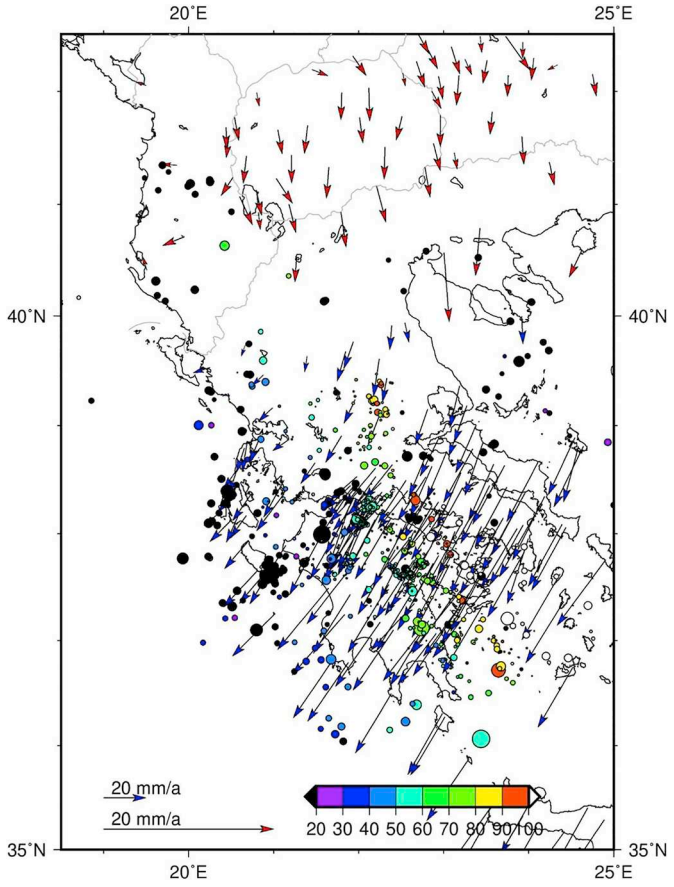

Fig. 3. GNSS-derived horizontal velocity field and seismicity. The velocities are relative to stable Europe, and are compiled from Jouanne et al. (2012), Nocquet (2012), and Metois et al. (2015). Please note that velocity vectors are 4 times larger for sites north of 40° N to allow better visualization. Epicenters for relocated earthquakes (Halpaap et al., 2018) are shown with circles, whose sizes are scaled with the magnitude and colored with depth.

Pec zone marks the boundary between the Dinarides and Hellenides, and defines the northern boundary of the high velocity zone at 150 km (Bijwaard and Spakman, 2000). To the north of the Scutari-Pec zone, the Adriatic slab does not penetrate below 150 km, whereas to the south of the zone slab is visible down to ~200 km depth (Handy et al., 2019). Towards the southeast, the slab penetrates to increasingly greater depths.

2.2. Other structural seismology studies

Recent research focused on investigating the structure of the Hellenic slab in the depth range from 50 to ~150 km (Suckale et al., 2009; Pearce et al., 2012; Sachpazi et al., 2016; Halpaap et al., 2018). Suckale et al. (2009) used coda waves of teleseismic earthquakes along a N60E-oriented seismic section below the Peloponnesus. They interpreted vertical fragmentation/tearing of the Hellenic slab below the Central Hellenic Shear Zone (Fig. 4B – STEP model). Pearce et al. (2012) deployed a dense array parallel to and 300 km north of the Peloponnesus seismic line and reanalyzed Suckale et al. (2009) data. They interpreted the structure between two profiles as a smooth ramp rather than a vertical tear (Fig. 4C – Ramp model).

Sodoudi et al. (2006) used receiver functions to conclude that the slab is continuous beneath northern and southern Greece down to ~200 km depth, in agreement with the ramp model in Fig. 4C. Evangelidis (2017) and Kaviris et al. (2018) interpret SKS splitting as evidence for toroidal flow below the KTF region and conclude that a tear exists between subducted slab fragments (Fig. 4B).

2.3. Seismicity studies

Halpaap et al. (2018) relocated regional earthquakes using double differences in combination with local traveltime tomography. They interpret their results as continental and oceanic subduction with a smooth transition across the KTF, i.e., in line with the ramp model. However, ray paths do not go deeper than 80 km beneath the KTF and its onland extension and lack information about sub-lithospheric depths. Combining tectonic reconstructions with the slab geometry retrieved from published seismological studies and hypocentral locations, Bocchini et al. (2018) proposed that the slab is segmented along the NE-ward prolongation of the KTF. According to Bocchini et al. (2018), the slab is unlikely to be detached at depths shallower than 100–120 km. Furthermore, Bocchini et al. (2018) calls for detailed tomographic work to further illuminate the slab architecture beneath the region.

The suggestion by Govers and Wortel (2005) that the KTF is a STEP can not be tested with published seismological results as a result of inconclusive information regarding fragmentation of the Hellenic slab. We aim to improve this using full-waveform tomography.

3. Data and methods

3.1. Tomographic inversion method

We use the S-velocity model from the full-waveform inversion of Fichtner et al. (2013). In contrast to the more widely used and computationally less expensive travel time tomography, full-waveform inversion naturally exploits all three-component body and surface waves in seismic recordings. Furthermore, the complete wave propagation physics in the 3D heterogeneous, attenuating and anisotropic Earth is correctly simulated numerically, thereby largely avoiding forward-

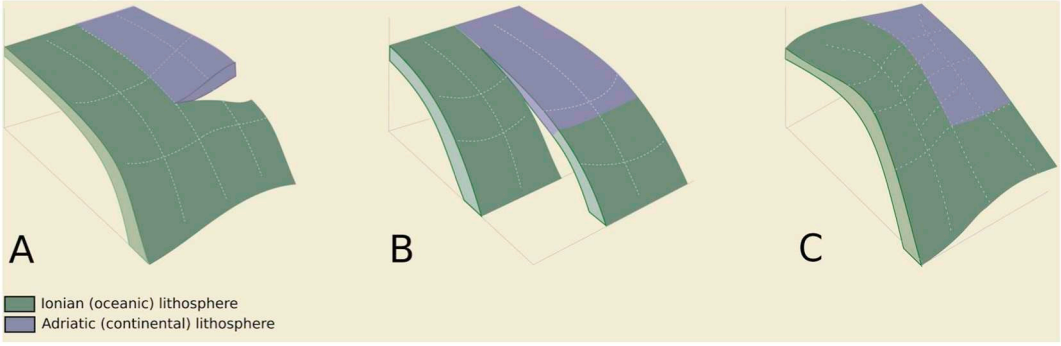

Fig. 4. Previous interpretations of the geometry of the western Hellenic subduction zone. A. Slab detachment (horizontal tear) model (Wortel and Spakman, 2000); B. Vertical/lateral slab tear model (Govers and Wortel, 2005); C. Smooth ramp model (Pearce et al., 2012).

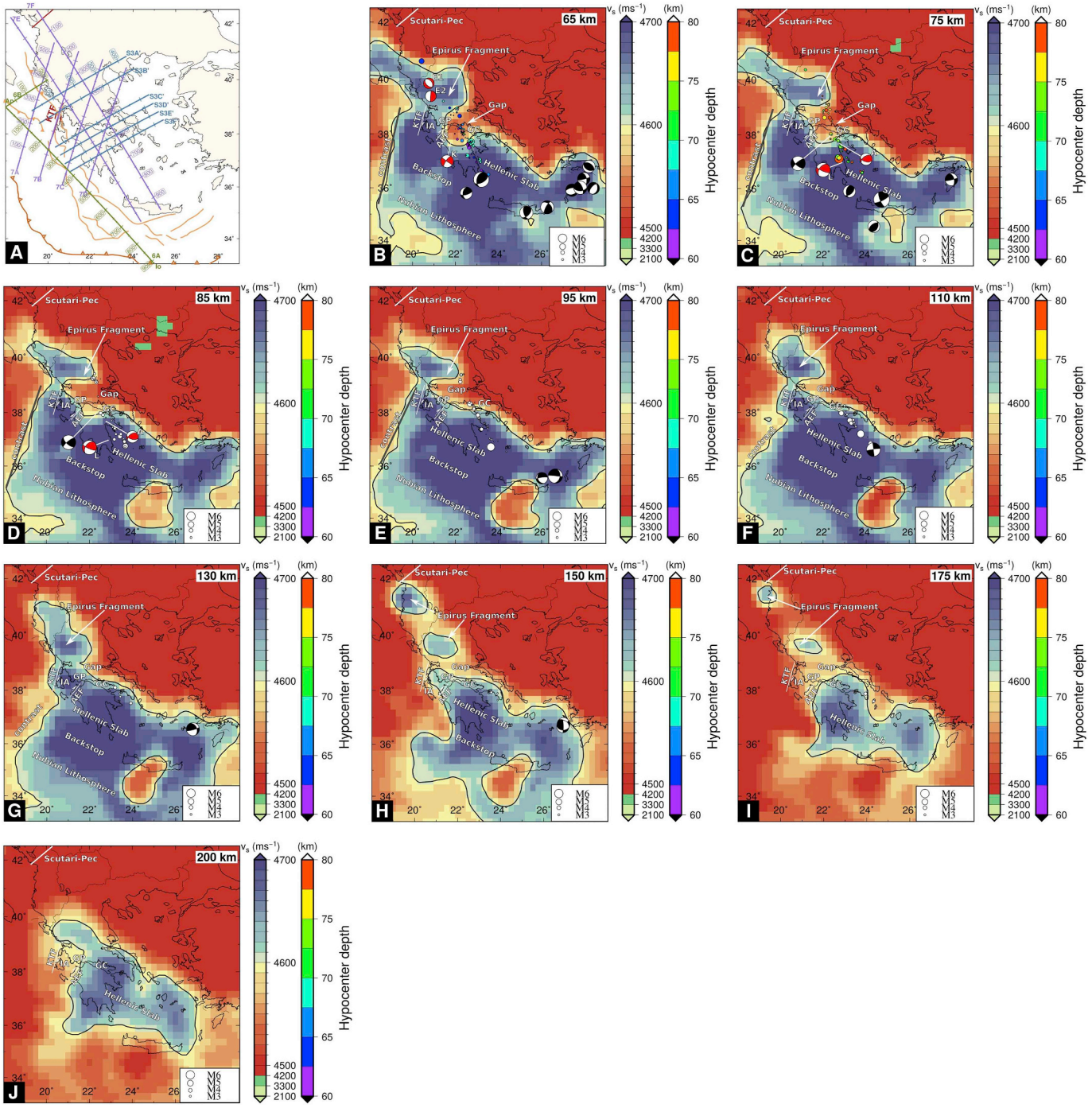

Fig. 5. A. Location map of vertical profile lines in Figs. 6, 7 and S3. Thin black lines show coastlines, the dark orange line is the trench, light orange lines represent faults, the red lines indicate the KTF and Scutari-Pec. (B-J) Horizontal section at 65, 75, 85, 95, 110, 130, 150, 175 and 200 km through the tomographic volume. Colors indicate isotropic S-wave velocities, the thick black line is the 4600 ms^{-1} contour. Please refer to Supplementary Fig. S4 for the same cross sections with an unsaturated color scale. Relocated earthquakes (Halpaap et al., 2018) are plotted when they occur within 5 km distance of a tomographic slice. Focal mechanisms of intraplate earthquakes within 10 km distance of a tomographic slice (Shaw and Jackson, 2010) are plotted in black. Red colored focal mechanisms (E_1, E_2, K, L, A) are discussed in the text. (For interpretation of the references to color in this figure legend, the reader is referred to the web version of this article.)

modelling artifacts. The combined effect of using full waveforms and accurate modelling is an improved resolution of Earth structure, especially in the 0–200 km depth range, where the majority of lithosphere-mantle interactions occur. The waveform data used to construct the model comprise 16,837 three-component seismograms, obtained from 113 earthquakes with magnitudes from 5.0 to 6.8 that occurred between 2005 and 2011 along the tectonically active margins of the Eurasian plate. Within the eastern Mediterranean region, complete seismograms were modeled and inverted in the period range from 8 to 200 s, ensuring that both crustal and upper-mantle structures are jointly constrained.

Quantitative analyses of tomographic resolution (Fichtner et al., 2013) indicate that S-velocity heterogeneities with a lateral extent of around 25 km or more are resolved from the surface to approximately 50 km depth. While a quantitative analysis of resolution length in vertical direction is technically more difficult, the comparison with

receiver function studies suggests that vertical resolution within the upper 50 km is around 10 km (Govers and Fichtner, 2016). Below 50 km depth, where the sensitivity of surface waves decays notably, both the lateral and vertical resolution length increases gradually.

3.2. Identification of intraslab earthquakes

We use M ≥ 4.5 earthquakes from the International Seismological Centre (ISC) Catalogue (Weston et al., 2018; Lentas et al., 2019) with the aim of constraining active deformation. The travel-time difference between direct P arrivals and the surface-reflected depth phase pP is particularly sensitive to the earthquake source depth (Lay and Wallace, 1995). For verification of the hypocentral depth relative to the upper plate Moho, we extracted six events with magnitude above 4.5 within a 2° radial distance from the KTF. For teleseismic distances, events with at least four pP and P readings and azimuths falling into two different quadrants are used to determine differential times per station distance. We compute characteristic distance-time curves using the TauP toolkit (Crotwell et al., 1999). The associated focal mechanism solutions are extracted from the ISC Catalogue and discussed in Sections 4 and 5.

4. Results

4.1. Displaying anomalies of isotropic S-velocities

Our tomographic model consists of anisotropic S-velocities ranging between 2500 and 4900 ms^{-1}. We focus on the upper 200 km of the model because here is where the most significant improvement relative to previous models may be expected. We first compute the isotropic S-velocity v_S from the velocities of horizontally (v_{SH}) and vertically (v_{SV}) polarized S waves, following Babuska and Cara (1991):

$$v_s = \sqrt{\frac{2}{3}v_{SH}^2 + \frac{1}{3}v_{SV}^2}$$

We compute relative velocity perturbations by selecting a reference mantle velocity that results in a slab structure that agrees best with the images of Bijwaard and Spakman (2000; BS2000) at 150 km depth (Supplementary Fig. S1). Our motivation for using their model is that it captures many of the features of other tomographic models with a regional focus (e.g., Koulakov et al., 2009; Zhu et al., 2015). Our reference mantle velocity is 4600 ms^{-1}, which is slightly higher than the ak135-F average S-velocity of 4500 ms^{-1} (Kennett et al., 1995). However, it falls well within the range of average uppermost mantle velocities for the Tethyan collision zone (Bastow, 2012; Govers and Fichtner, 2016). Halpaap et al. (2018) find an average S-velocity of 4600 ms^{-1} below 60 km in their local model. In the next section we present horizontal sections from select depths with the same reference velocity and color scale for the mantle. The same cross sections with an unsaturated color scale can be found in Supplementary Fig. S4.

4.2. Horizontal sections

Fig. 5H shows the S-wave perturbations at 150 km depth with the same color scale as BS2000 (Supplementary Fig. S1). The northeastern limit of the interface between the Hellenic slab and the mantle wedge agrees largely for the two models. Arc-perpendicular slab widths compare well, too. The topologies of the southwestern limit of high-velocity anomalies below the Ionian basin differ. This is likely caused by better imaging of the thick oceanic lithosphere by surface waves in our model. A significant difference —and the focus of our study— is that the northwestern part of the Hellenic slab is fragmented, whereas it was imaged as a continuous feature by BS2000. It should be emphasized, however, that apart from using different data and techniques, we also analyze different physical quantities, i.e., P and S velocity. For this reason, tomographic images can deviate significantly from each other. A low-velocity gap below continental central Greece near Kefalonia suggests a lateral discontinuity in the slab structure. Another discontinuity is imaged to the north of 40° N. Our tomographic model at 150 km depth thus suggests the existence of a separate slab fragment below Epirus. In the following discussion we refer to this fragment as the Epirus fragment.

The section at 65 km depth (Fig. 5B) cuts horizontally through the Nubian lithosphere and its subducting part, the Hellenic slab, and into either the asthenosphere below the overriding plate, or into its lithospheric mantle. Beneath the west Aegean Sea, the thick contour line represents the NW striking contact between the Hellenic slab and the mantle wedge beneath the thin Aegean lithosphere. This contour wraps around GC and northern Peloponnesus, and outlines a low-velocity zone that we interpret as a gap between the Hellenic slab and the Epirus fragment. A roughly rectangular high-velocity anomaly protrudes from Epirus towards southern Albania and Italy. Larger (M > 4.5) events with a focal mechanism are clearly located within either the Hellenic slab, or within the Epirus fragment. Hypocenters of the majority of the earthquakes M > 3 are located within the Hellenic slab also. Smaller (M < 3.0), and therefore possibly less well located, events plot into the low-velocity gap, which is located in the western end of GC and northern Peloponnesus.

At 75 km depth (Fig. 5C), the Epirus fragment is smaller than in the section at 65 km. The gap widens towards the NE and thus reaches the northern end of the KTF. Relocated seismicity is mostly in agreement with the velocity structure, although there is a streak of M ~ 3 events trending NNW within the northern part of the GC. The NW-SE extent of the Epirus fragment gradually gets smaller with depth (Figs. 5D, E), and from 85 km and deeper it is confined mainly beneath the land areas. The location and geometry of the gap in the 85 and 95 depth sections are very similar to that in the 75 km section. Seismicity is concentrated near the SE corner of the Epirus fragment and within the Hellenic slab. In the NW part of the Ionian basin we image a contrast between high and low-velocity anomalies that roughly aligns with the strike of the KTF, and that is parallel to the rollback direction of the trench. The location of the transition coincides with a gradient in free-air anomalies (Tugend et al., 2019), suggesting that it represents a lithospheric compositional contrast.

At 110 km depth, the main high-velocity anomaly extends to the SW into the Ionian ocean basin (Fig. 5F). The oceanic lithosphere of the Ionian basin is of Mesozoic age, and possibly ~225 Ma old (Speranza et al., 2012). Therefore, it is likely thicker than 100 km, and we will see below that the Ionian/Nubian lithosphere is thicker than 150 km in places. The low-velocity gap below continental central Greece is not apparent at this depth. The Epirus fragment and the gap appear in the same location and have a similar geometry as at 85 and 95 km depth.

The horizontal section at 130 km depth (Fig. 5G) shows a shift towards the NE of the 4600 ms^{-1} contour below continental Greece relative to the 110 km location. This shift reduces the size of the gap substantially. The Epirus fragment extends further to the NW. At 150 km depth the gap between the Epirus fragment and the Hellenic slab is reestablished, and the Epirus fragment appears to have fragmented itself (Fig. 5H). The size of the high velocity anomaly associated with the Nubian/Ionian lithosphere has further decreased.

Two Epirus fragments are visible at 175 km depth (Fig. 5I). This horizontal section is mostly located below the Nubian/Ionian lithosphere. The Hellenic slab is confined below the Peloponnesus and the south Aegean region. The wide cross-sectional dimension of the Hellenic slab gives a false impression of the actual slab thickness because of the low slab dip (Bijwaard et al., 1998). The slab-wedge interface is oriented NW-SE. The tomographic section at 200 km depth suggests that the Epirus fragment is continuous with the Hellenic slab (Fig. 5J).

The tomographic model also includes the crust. Supplementary Fig. S2 shows a horizontal section at 15 km depth. Contrasts in crustal structure in the overriding plate show little correlation with tectonics maps or with major crustal faults.

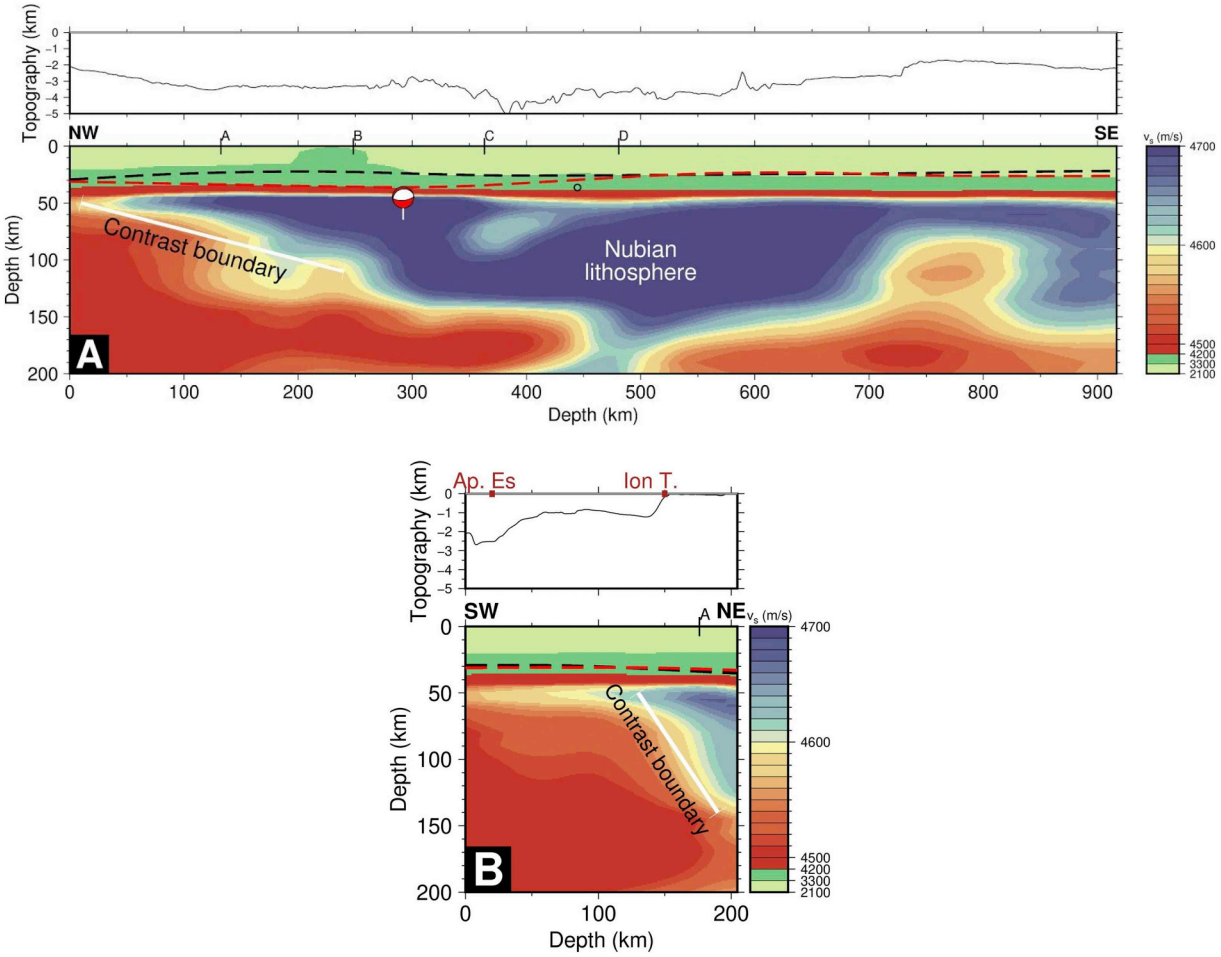

Fig. 6. Cross-sections through our S-velocity volume, see location map 5A. A. Ionian/Nubian lithosphere and asthenosphere B. Apulian escarpment. Letters on top of the panels indicate intersecting profiles. Red and black dashed lines show the crustal thickness variations from CRUST1.0 (Laske et al., 2013) and Karabulut et al. (2019) respectively. Open circles and focal mechanisms represent epicenters of earthquakes within a horizontal perpendicular distance of 25 km of the cross section. Please refer to Supplementary Fig. S5 for the same cross sections with an unsaturated color scale. (For interpretation of the references to color in this figure legend, the reader is referred to the web version of this article.)

4.3. Cross sections

We use the same color scale for the mantle in vertical sections as in horizontal sections. We extended the color scale with tones of green to include low S-velocities in the crust. Cross sections with a non-saturated color scale are shown in Supplementary Figs. S5 and S6. Our tomographic model does not show a sharp Moho in the sense of an exact discontinuity in seismic velocities. Instead, higher mantle velocities gradually transition into lower crustal velocities. Most importantly, this ensures that the sharpness of the crust-mantle transition is fully controlled by the actual data that enter the inversion. This is in contrast to more conventional seismic tomography where a discontinuous Moho is fixed a priori, thus introducing the risk that imperfections of the crustal model leak into spurious upper-mantle structure. While being highly beneficial from a technical tomographic perspective, our approach comes with the disadvantage of a less straightforward separation of crust and mantle during the interpretation of the model. Based on the frequency content of the waveform data included in the inversion, we estimate that the sharpest possible crust-mantle transition in our model is around 10 km thick.

Fig. 6A shows a cross section through the Nubian lithosphere and asthenosphere along profile Io in Fig. 5A. The thickness of the shallowest low-velocity layer of ~35 km is remarkably constant. This layer consists of both sediments of the Mediterranean Ridge (about 10 km thick, Fruehn et al., 2002), and of the underlying crust. The contrast that we noted in the horizontal slices 65–130 km depth is clearly visible in the sub-crustal mantle in the northwestern part of the cross section. The lithospheric contrast dips to the southeast over a horizontal distance of 300 km. A simple interpretation would be that the lithosphere is surprisingly thin (~50 km) in the northwest, and substantially thicker (~150 km) to the southeast, which is more in line with what may be expected for Mesozoic oceanic lithosphere (Burgos et al., 2014).

Fig. 6B is a cross section across the Apulian Escarpment along profile line Ap (Fig. 5A). The crustal thickness (and structure, c.f. Supplementary Fig. S2) varies little and is about 30 km, which differs from the sharp contrast in the upper crust (e.g., Tugend et al., 2019). There is a significant contrast in the lithospheric mantle structure, but it is offset relative to the Apulian Escarpment by ~100 km to the NE. One interpretation of the anomalies would be that the lithosphere is thin on the Ionian Sea side (~50 km) and relatively thick (~140 km) on the Adriatic side of the Apulian Escarpment. The lateral variability of this thickness contrast can be appreciated from the horizontal slice at 110 km, which shows that the contrast is absent further to the WNW; Below easternmost Apulia we find a lithospheric thickness of ~80 km, which agrees with the result from receiver functions below onshore seismological station SCTE by Miller and Piana-Agostinetti (2011).

Cross sections in Fig. 7A–D are taken parallel to the present-day rollback direction of the trench relative to Africa (Nocquet, 2012) as indicated in Fig. 5A with labels A-D. Alternative cross sections perpendicular to the trench as in Halpaap et al. (2018) (Fig. 5A, labels A'-

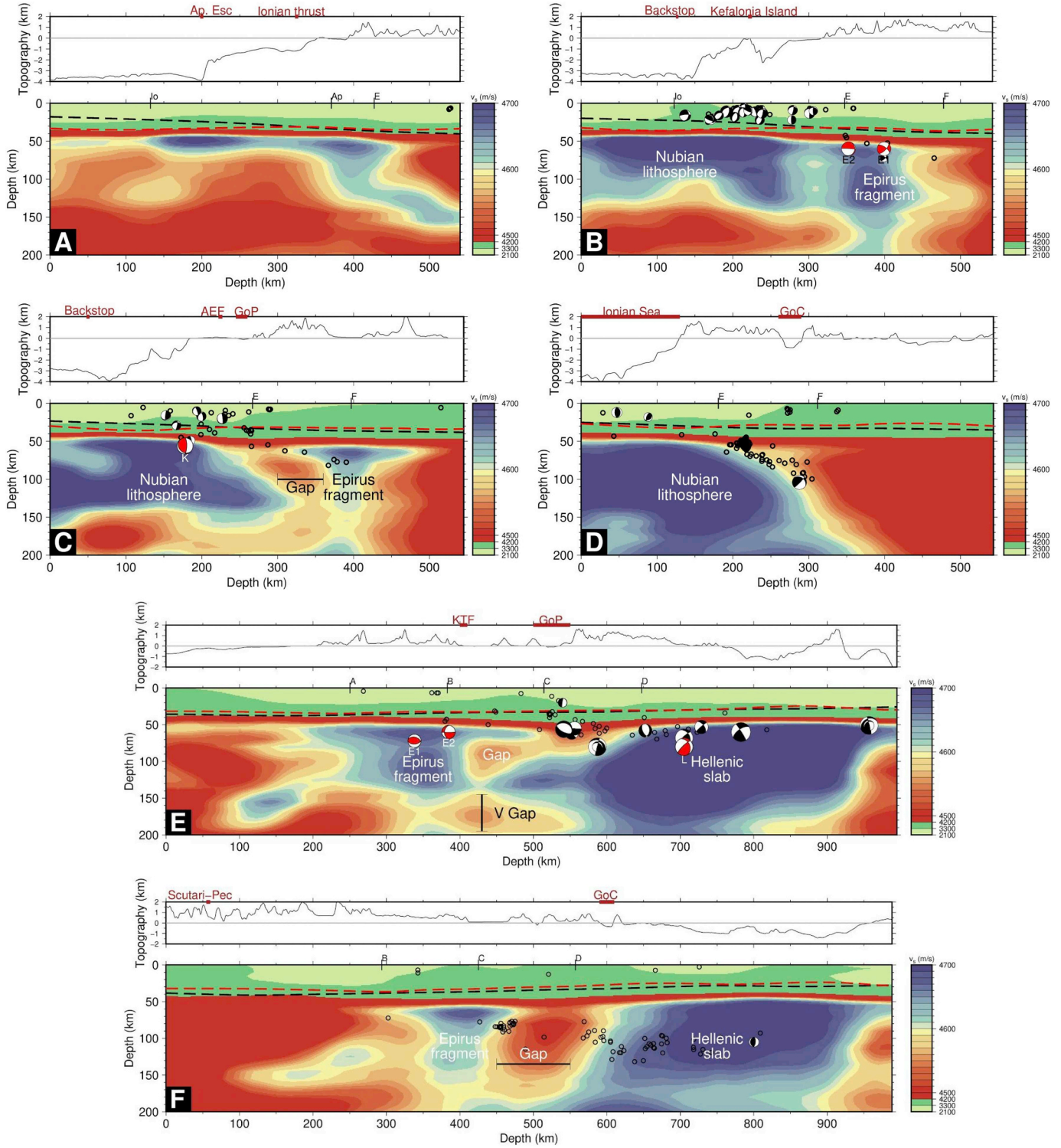

Fig. 7. Vertical sections along the present-day rollback direction of the trench (sections A-D), and in a direction that is approximately parallel to the Western Hellenic Subduction Zone (sections E–F). The map panel shows where the cross sections are taken, and red and white circles on the cross section lines indicate 250 km intervals. On cross sections (A–F), red inverted triangles are used to indicate surface locations of the KTF and the Gulf of Corinth. Letters on top of the cross sections refer to the intersecting profiles. White open circles represent M > 4 events, taken from the ISC, that have hypocenter errors (both vertical and horizontal) ≤10 km. Hypocenters within a swath of 50 km are projected onto the profiles. Red and black dashed lines show the crustal thickness variations from CRUST1.0 (Laske et al., 2013) and (Karabulut et al., 2019) respectively. Please refer to Supplementary Fig. S6 for the same cross sections with an unsaturated color scale. (For interpretation of the references to color in this figure legend, the reader is referred to the web version of this article.)

F′) are shown in Supplementary Fig. S3. In the SSW, section 7A cuts into the thin lithosphere below the Ionian basin (c.f. Fig. 5 at 75 km). The high-velocity anomaly in the NNE (375–550 km) extends to ~150 km depth. This anomaly represents the northwesternmost part of the Epirus fragment.

Vertical section 7B shows the thick Nubian lithosphere below the Ionian basin in the SSW. The amplitude of the fast velocity anomaly between 60 and 130 km depth is lower near the coast of the mainland

(horizontal distance of 300 km). Inspection of the horizontal sections shows that this cross section is located close to the low-velocity anomaly that separates the Hellenic slab from the Epirus fragment, which is visible further to the NNE between 350 and 450 km distance. The Hellenic slab as imaged in previous tomographic studies (e.g. Bijwaard and Spakman, 2000) at greater depths is not visibly connected to the Nubian plate below the Ionian basin in this section.

Cross section 7C shows a clear separation (gap) between the (thick) Nubian lithosphere beneath the Ionian basin and the Epirus fragment above 130 km depth. The Nubian lithosphere is not connected with a deeper Hellenic slab. The NNE edge of the underthrusted Nubian lithosphere has a dip that agrees with the Sachpazi et al. (2016) results.

Cross section 7D shows continuity of the Nubian lithosphere into the Hellenic slab. The horizontal sections show that subduction presently occurs between Messenia and western Crete. Seismicity correlates well with the imaged top of the slab.

Fig. 7E is a cross section parallel to the coastline (Fig. 5A). In the NW, it shows continental lithosphere (0–200 km distance) adjacent to the Epirus fragment. The NW edge of the Epirus fragments coincides with the Scutari-Pec fault zone in the overriding plate. The low-velocity region between the KTF and the continuous part of the Hellenic slab indicates that the Epirus fragment is a separate feature. A ~ 50 km vertical gap appears to exist between the downward end of the Epirus fragment and deeper Hellenic slab anomalies.

The horizontal separation between the Epirus fragment and the Hellenic slab is even more pronounced in cross section 7F. It is not entirely clear whether the high-velocity anomalies merge below 150 km depth, i.e., the vertical gap is not apparent in this cross section.

5. Connection between structure and kinematics

5.1. Seismicity in the Hellenic slab and Epirus fragment

The hypocenter and focal mechanism of the Mw 6.4 Leonidio earthquake were constrained by Zahradnik et al. (2008) and Kiratzi and Benetatos (2008). Sachpazi et al. (2016) report a hypocentral depth of 70 km, whereas the centroid depth according to Pondrelli et al. (2011) is at 87 km. Our analysis suggests a depth of 80 km (Fig. 8). The earthquake is located well within the Hellenic slab (event marked with "L" in Figs. 5C–D and 7E). Sachpazi et al. (2016) interpret it as an intraslab event as part of fragmentation of the Hellenic crust.

The hypocenter (depth = 70 ± 10 km) and focal mechanism of the 2008/06/18 Mw 5.0 Argos earthquake were constrained by Pondrelli et al. (2011) and Sachpazi et al. (2016). Our plot of pP-P differential times versus epicentral distance (Fig. 8) suggests a hypocentral depth of 60 km. In our structural interpretation, the event is located within the shallow part of the Hellenic slab (label "A" in Figs. 5C, D). Sachpazi et al. (2016) select the NW dipping nodal planes as the intraslab fault and interpret it as a left-lateral transpressive event as part of fragmentation of the Hellenic crust.

The 2008/06/30 Mw 4.6 "Epirus 2" earthquake (ISC Event #13378954, Pondrelli et al., 2011) occurred below the Epirus region. Our plot of pP-P differential times versus epicentral distance (Fig. 8) suggests a hypocentral depth of 60 km. This means that the event was located 20 km below the Moho of the overriding plate, along the edge between the Epirus fragment in the north, and the low-velocity anomaly in the south (Figs. 5B and 7B). We suspect that the horizontal nodal plane represents the fault plane. The reason is that the vertical nodal plane aligns roughly with the seismic velocity contrast which probably also represents a strength contrast. This we consider an unlikely candidate fault plane because it is difficult to accumulate shear stresses when one block alongside a fault is weak. Our interpretation implies that this event represents westward thrusting over the Epirus fragment of the crust of the overriding plate.

The 2003/12/07 Mw 4.5 "Epirus 1" earthquake (ISC Event #7201105, Pondrelli et al., 2007) occurred below the Epirus region at a depth of ~60 km (Fig. 8). This means that the event was located well within the Epirus fragment (Figs. 5B and 7B). The focal mechanism corresponds to horizontal NE–SW oriented horizontal tension, or vertical compression. These principal stress directions diverge strongly from orientations for other events in the region, suggesting that the Epirus fragment experiences little slab pull, possibly indicating that it is not connected to the deeper Hellenic slab.

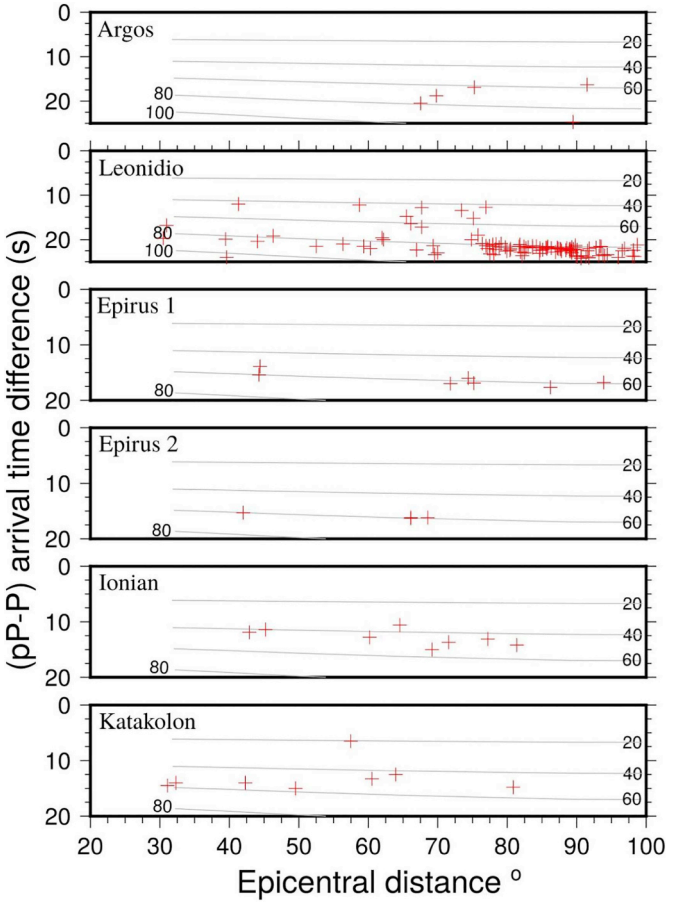

Fig. 8. Delay time of P- and pP-phases are plotted against distance between stations and the event. Dashed gray lines show the characteristic depth at which phase difference and separation correspond.

The June 111,999 Mw 5.2 strike-slip earthquake occurred offshore northwestern Peloponnesus (ISC Event #1665492, denoted by Katakolon in Fig. 8 and with the letter "K" in Figs. 5B and 7C). pP-P travel time differences indicate a depth of ~50 km (Fig. 8), which is consistent with the ISC estimate. The centroid depth according to Pondrelli et al. (2011) is 65 km. We take the latter value as a deeper limit and thus suggest that the Katakolon earthquake occurred between 50 and 65 km depth. The event is therefore located in the topmost part of the underthrusted Nubian lithosphere. If we interpret the NE-striking nodal plane as the fault plane, the mechanism indicates left-lateral shear. This interpretation is in agreement with the mechanisms of Leonidio and Argos events, both of which exhibit sinistral slip but with a larger oblique component. Furthermore, the NE-striking nodal plane is in agreement with dominant NE-SW trending intraplate events for the western Peloponnesus (Fig. 5; relocated seismicity from Halpaap et al. (2018)). The fault plane responsible for the Katakolon earthquake should be one of the intraslab faults (F2 of Sachpazi et al., 2016) as part of fragmentation of the Hellenic crust.

5.2. Seismicity along the Kefalonia Transform Fault

The vast majority of the strike-slip seismic activity along the KTF

(Baker et al., 1997) corresponds to dextral slip between the Nubian lithosphere and the forearc (Kassaras et al., 2016). Based on the seismicity, it is uncertain whether the slab tear (that we identify as a gap from the tomography) also has an expression in the overriding lithosphere. The accretionary wedge and foreland are clearly offset, but particularly the landward continuation of a potential STEP fault into the overriding plate is unclear. We will return to this topic in Section 5.4.

5.3. Plate boundary seismicity

Beneath the Ionian Islands thrust faulting earthquakes strike oblique to the plate boundary, in a N−S direction, and their slip vectors are almost perpendicular to that of GNSS velocities (Shaw and Jackson, 2010).

The October 52,010 Mw 4.7 earthquake in the Ionian basin, SW of Zakynthos island (ISC Event #7415293) occurred at ~45 km depth according to pP-P travel time differences in Fig. 8. With reference to the tomographic profiles, this event is located along the interface between the Hellenic slab and the overriding plate (Fig. 6A, denoted by letter "I"). Nevertheless, this event differs from nearby interface events because of its larger depth. Hirn et al. (1996) suggested that the shallow dipping interface between the Nubian lithosphere and the overriding plate beneath the Ionian Islands is at 13 km depth. However, according to Shaw and Jackson (2010), the depth of interface earthquakes can vary in a large-range, between 15 and 45 km. Therefore, we interpret this event as an interface earthquake in response to the convergence between the Nubian lithosphere and the overriding Aegean.

5.4. Active deformation of the overriding plate

Fig. 9A shows crustal seismicity and active faults in the overriding plate and plate boundary zone. The rate of seismic moment release increases significantly from the NW to the SE. Fig. 9B shows the regional-scale zonation into compressional, strike-slip and extensional deformation. This zonation is based on focal mechanism solutions, on the analysis of seismicity patterns, and on the classification of active and recent faults (Basili et al., 2013; Handy et al., 2019). Below, we discuss these tectonic zones.

In the southern Dinarides close to the Adriatic Sea, focal mechanisms document distributed thrusting within the overriding plate (Baker et al., 1997; Pondrelli et al., 2006, 2011; Copley et al., 2009) with azimuths of reverse slip vectors that are consistent with GNSS-derived velocity directions (D'Agostino et al., 2008). The convergence is accommodated mainly by frontal low-angle thrusts and shortening in the external Dinarides (Korbar, 2009; Biermanns et al., 2019).

Fig. 9B shows that active tectonics substantially change near the Scutari-Pec line at the transition from Dinarides to Albanides. Volumetric strain rates from GNSS velocities indicate that the Scutari-Pec region represents the boundary between compressional (N) to tensile deformation (S), and that it involves moderate clockwise vertical-axis rotation rates, and moderate bulk shear strain rates (Perouse et al., 2012; Metois et al., 2015).

Further to the SSW, seismic activity in the forearc is clustered along mapped thrust faults in Albania (Fig. 9A). Further away from the plate contact, crustal earthquakes in the internal part of the Albanides show E-W extension (Jouanne et al., 2012). A significant horizontal dilatation rate is inferred for the eastern Albanides from GNSS data (Metois et al.,

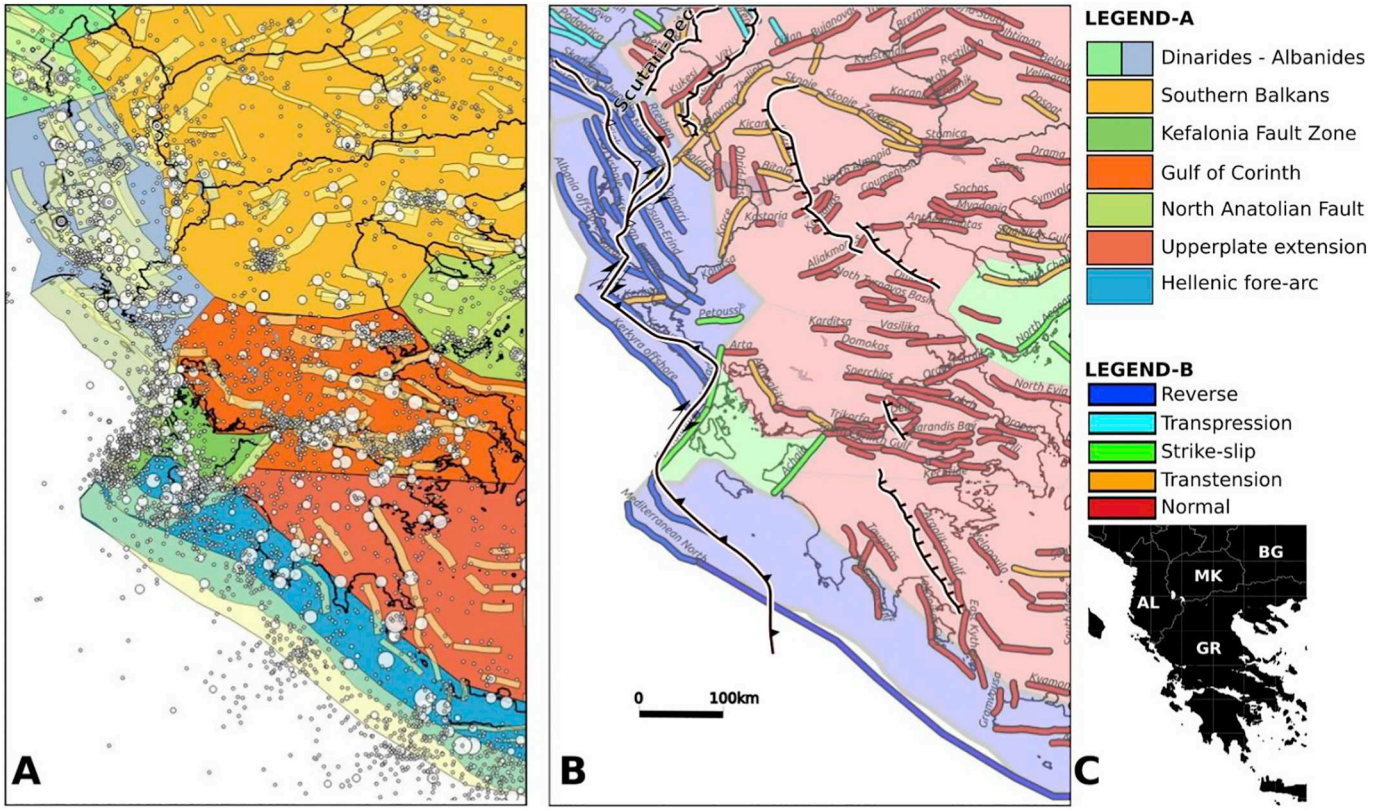

Fig. 9. Active faults in the overriding plate and along the plate contact zone. A. Seismogenic zones and faults modified from SHARE (The European database of Seismogenic Faults, Basili et al., 2013). Light yellow bands show surface projections of seismogenic faults, white circles show epicenters of M4+ earthquakes. Background colors show seismotectonic regions (legend-A). Black lines show coastlines and national boundaries. B. Zonation of recent tectonic activity from combining seismogenic and Neogene faulting is shown by fill colors (Legend-B). Fault names are from the SHARE database. Neogene faults are shown by black lines with white background (Handy et al., 2019). C. National borders of Balkan countries and Greece are mentioned in the text (GR:Greece, AL:Albania, MK: North Macedonia; BG: Bulgaria). (For interpretation of the references to color in this figure legend, the reader is referred to the web version of this article.)

2015). The Albanides separate the region of NE-ward GNSS convergent motions in the W from the region in the E with S- to SW-ward motions of the overriding plate. GNSS velocities increase in magnitude towards E and S, but the overall motion is compatible with a clockwise rotation pattern (Fig. 3). Relative to the northern Albanides, thrust activity may be more concentrated closer to the trench, suggesting a SE ward transition from shortening to subduction.

The southern Balkan crust moves southward towards the Hellenic subduction zone in a Eurasian reference frame (McClusky et al., 2000) at a slow rate of 3 mm/yr (Burchfiel et al., 2006; Kotzev et al., 2006; Nocquet, 2012) (Fig. 3). GNSS-derived horizontal dilatation rates (Metois et al., 2015) and neotectonic fault activity indicate transtension. The zonation of active faults (Giardini et al., 2014, Fig. 9) corroborates the GNSS-derived deformation pattern; there is an abundance of normal faults which strike ENE to ESE, and way fewer transtensional faults with NW-SE strikes. In Fig. 9B, this extensional zone continues into the Peloponnesus and Aegean region. GNSS velocity gradients are low in the southern Aegean region (Fig. 3), as are the resulting dilatation and shear strain rates (Chousianitis et al., 2015). Extension focuses mostly in the Peloponnesus. The horizontal extension direction changes within short distance, from E-W extension in the center and south, to NE-SW in the west (Kreemer et al., 2004; Chousianitis et al., 2015). NNW-striking normal faults were mapped in the field (e.g., Papanikolaou and Royden, 2007; Papanikolaou et al., 2007), which agree with the seismogenic zone delineated in Fig. 9. The zone of active and recent normal faulting is thus continuous from the Balkan to the south Peloponnesus.

The transpressive KTF *zone,* bounded by the KTF and the Achaia-Elia fault (Fig. 2 and Fig. 9B) is seismically very active. The KTF accommodates dextral slip (Baker et al., 1997; Louvari et al., 1999) along the northwest boundary of the KTF zone. The Achaia-Elia fault also shows dextral slip (Ganas and Parsons, 2009; Vassilakis et al., 2011; Kassaras et al., 2016). Between these bounding faults the KTF zone is seismically much less active. Shallow seismicity (< 30 km depth; Kassaras et al., 2016) along the KTF shows differential motion between the crust of the Ionian basin and the crust of the Hellenic forearc. Importantly, transpressional activity terminates abruptly to the northeast, where the KTF comes onland. This means that there is no localized, seismically active shear zone within the overriding plate beyond the KTF. Seismicity along the Achaia-Elia fault shows an opposite behavior; the seismically active fault is restricted to the overriding plate, and does not continue into the forearc (Ganas and Parsons, 2009; Kassaras et al., 2016). The northern end of the Achaia-Elia fault terminates near the GC. Below, we discuss the downward continuity of the Achaia-Elia fault into the Hellenic slab. So, the KTF zone accommodates distributed dextral transpression between the Ionian basin and the overriding plate. The KTF zone has a limited extent towards the northeast (Fig. 9B).

Considering the prolongation of the KTF zone towards the northeast, we need to discuss the suggestion of Papanikolaou and Royden (2007) that the dextral motion of the North Anatolian Fault/North Aegean Trough continues to central Greece through the transtensional "Central Hellenic Shear Zone" (CHSZ). CHSZ includes the Gulf of Corinth and ultimately joins with the Hellenic trench via the KTF. The seismic moment release, geodetic strain rates, and faulting indeed clusters in their CHSZ. If the NAT and KTF would form a pull-apart, then the deformation would be concentrated to the north of ~39 N and normal faults would strike between E-W in the west and WNW-ESE in the east. The normal faults within the Gulf of Corinth and those forming the active southern flank strike E-W, thus the orientations roughly agree. However, the location of the Corinth Rift is much more to the south, which refutes the shear zone interpretation. On the other hand, if the AEF would be involved in the step-over then the region between would be under compression. Thus, AEF cannot be part of a releasing step-over. Alternatively, in a typical simple shear experiment, until the post-peak period, only the R- and R'-shears form. If the CHSZ, including the GC and other half-grabens would have formed as "tension gashes", the synthetic and antithetic faults would be expected to have been previously active. For the North Anatolian Shear Zone, Şengör et al. (2005) describe the formation of tension gashes in the post-peak stage by lengthening of R-shears" and the linking tension gash segments may develop into true pull-apart basins." For the proposed CHSZ we do not see an earlier stage in which such a connection occurs. Chousianitis et al. (2015) conclude that there is no geodetic evidence for the NAF Zone entering mainland Greece. Furthermore, the focal mechanism solutions in mainland Greece exclusively show normal faulting (Kiratzi and Louvari, 2003), no strike-slip. This is also demonstrated in the seismic zone boundaries of Fig. 9B, where the zonation shows that the shear deformation zone does not reach the mainland. We therefore conclude that the KTF zone has a limited extent and is not a fully developed shear zone connecting to NAF. We think that it is entirely likely that this will happen in the future as rollback of the Aegean trench continues, which is why we refer to the KTF zone as a proto-STEP fault.

5.5. Synthesis

The current kinematics of the overriding plate, deformation within the slab, and along the plate interface, offer a qualitative understanding of the coupling between the Hellenic slab and the upper plate. The KTF zone is a proto-STEP fault that is situated near the northwestern end of the gap between the Hellenic slab and the Epirus fragment (Figs. 5B, C, and D).

Fig. 10A shows a synoptic view of the imaged structure. The Epirus fragment is a roughly vertical feature below the southern Albanides. It is separated from the Hellenic slab by a horizontal gap (Fig. 5). Tomographic results for the deeper upper mantle (Van der Meer et al., 2018) show that the Hellenic slab is located beneath the Albanides, but does not extend to the northwest beyond the Scutari-Pec fault zone (Fig. 9B; Handy et al., 2019). A vertical gap (Fig. 7E, F) may exist between the Epirus fragment and the deeper Hellenic slab, and downdip shortening during the Epirus 1 earthquake (Section 5.1), i.e., absence of a slab pull signature, supports this interpretation. The vertical size of the gap between the down dip end of the Epirus fragment and the deeper Hellenic slab is estimated from Fig. 7E to be 45 ± 15 km. To estimate the time that was needed to develop this gap we assume that the Epirus fragment was connected to the deeper Hellenic slab prior to slab detachment, and that the shallow-dipping Hellenic slab subsequently rolled back to its present location. We assume also that the Epirus fragment stalled so that the slab gap was entirely caused by the rollback of the Hellenic slab (Fig. 10). The average trench migration rate was 20 ± 3 mm/yr during the Pliocene (Royden and Papanikolaou, 2011)). The average dip of the Hellenic slab dip was ~30°–17° in the depth range 20–100 km (Pearce et al., 2012) and 45° between 100 and 180 km (Papazachos et al., 2000). The time required for the development of the observed slab gap would be $\frac{45 \pm 15}{tan\ 30 \times 20 \pm 3}$ = 3.9 ± 1.3 Ma.

6. Evolution of the Western Hellenic active margin

6.1. Geological evolution of the main tectonic elements in the overriding plate

6.1.1. Regional context

Oligocene to Miocene development of a gap in the Hellenic slab below the northern and central Dinarides is commonly argued based on the absence of high-velocity anomalies (Wortel and Spakman, 2000; Faccenna et al., 2014; Handy et al., 2015; Le Breton et al., 2017). Consequently, there would have been some sort of lateral edge along the Hellenic slab to the north of Epirus during the period prior to the fragmentation of Epirus. Importantly, there is no evidence of STEP fault activity in the overriding plate during this period. As we will discuss in Section 6, the absence of STEP faulting during the Late Miocene may be

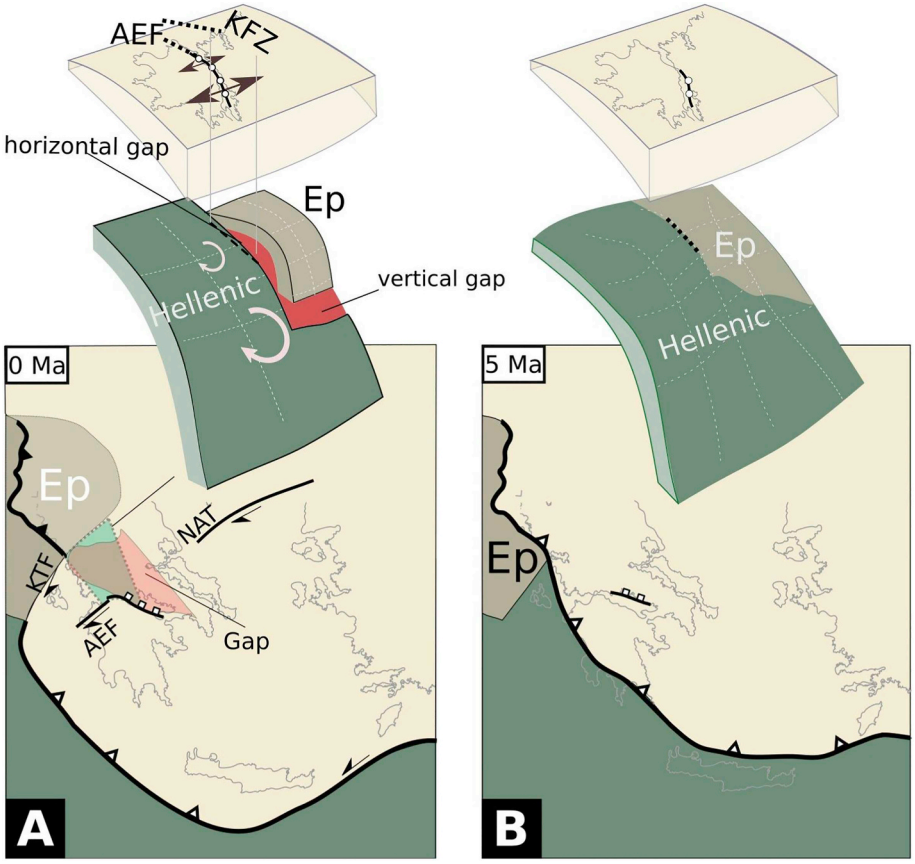

Fig. 10. A. Summary block diagram of our interpretation of the structure of the west Hellenic subduction zone and the Epirus fragment, present-day B. Tectonic setting of the Hellenic slab and the overriding plate deformation, 5 Ma. Circular arcs with arrows indicate sagging/rotation of the subducted slab.

related to the predominantly dextral relative motion of Adria and Moesia.

Miocene tightening of the orogen continued in the northern Hellenides until the Apulia continental margin collided with the European margin in the northern Hellenides, whereas to the south, the subduction continued to the south of the current location of the KTF (Royden and Papanikolaou, 2011). Paleomagnetic studies document ~50° of clockwise rotation of the larger region from Albanides and Hellenides with respect to the Dinarides (Kissel et al., 1995), of which 40° occurred between the middle to late Miocene and the remaining 10° occurred after 4 Ma (Van Hinsbergen et al., 2005; Van Hinsbergen and Schmid, 2012). In the internal part of the Hellenides of mainland Greece, NW-SE striking low-angle normal faults developed between the late Miocene, early Pliocene times, parallel to and possibly using the inherited weakness zones of the earlier nappe emplacement (Papanikolaou and Royden, 2007). Since early Pliocene times, E-W striking high angle normal faults obliquely cut earlier nappes and low-angle normal faults (Papanikolaou and Royden, 2007). The sense of shear on active faults in the Hellenides thus changed significantly since the Miocene likely in response to changes in the regional stress field from dominantly NE-SW extension to N-S extension during the Plio-Pleistocene epoch (Meijer and Wortel, 1996, 1997). It was in this regional context that the KTF became active.

6.1.2. Kefalonia Transform Fault Zone

The age of KTF has been argued primarily on the basis of geological and paleomagnetic data. One primary age constraint is that the fault post-dates the latest stage of nappe-emplacement in western Greece. Thrust faults of Messinian age (~5–7 Ma) are continuous in mainland Western Greece (Royden and Papanikolaou, 2011). However, west of the Ionian Thrust in Zakynthos, compressional deformation affected Messinian evaporites, which are unconformably overlain by Pliocene sediments (Underhill, 1989). Early Pliocene shortening near Lefkas, Kefalonia and Zakynthos likely reflect overthrusting of Ionian units on the Pre-Apulian zone (Clews, 1989). Underhill (1989) restored structural cross-sections in the island of Kefalonia and tentatively demonstrated that westward advancing thin-skinned tectonics continued well through the Pliocene and Pleistocene. All this evidence lends support to the early Pliocene final emplacement of the Ionian unit.

Van Hinsbergen et al. (2006) reported a renewed uplift of at least several hundreds of meters in the Pleistocene from paleobathymetry data and propose that the deformation along the KTF is responsible for this. Furthermore, they relate ~20° late-Pleistocene clockwise rotation (Duermeijer et al., 1999), to dragging along the KTF (Van Hinsbergen and Schmid, 2012). In Zakynthos particularly no significant rotation was recorded between 8.11 and 0.77 Ma, then the island underwent a 21.6° ± 7.4° clockwise rotation from 0.77 Ma to present (Duermeijer et al., 1999). No significant paleomagnetic rotation seems to have occurred since ~1.9 Ma along the SW coast of Kefalonia (Duermeijer et al., 2000). Onshore of Zakynthos in the NW edge of the Peloponnesus, very large rotations similar in magnitude to that of Zakynthos were demonstrated (Duermeijer et al., 2000).

This intensification of deformation may indicate that the localized fault should have emerged in the Pleistocene. Consistent with this interpretation, Reilinger et al. (2010) suggest that ~60 km offset on the KTF would put its age at 2 Ma, assuming present-day geodetic rates. Royden and Papanikolaou (2011), suggest a post-Messinian or early-Pliocene age for the inception of the KTF. Their geodynamic modelling results suggest an age of 4 Ma. After this, the thrust front migrated to its present location between the oceanic Ionian basin and the pre-Apulian continental shelf, thereby facilitating the latest oceanic subduction phase.

Van Hinsbergen et al. (2006) and Van Hinsbergen and Schmid (2012) emphasized the role of the dextral Thesprotiko fault zone, which has been considered the now inactive on-land continuation of the KTF. They suggest that the Thesprotiko fault zone accommodated the deformation in western Greece relative to the stable northern parts, between 7 Ma and pre-rifting in the Gulf of Corinth. Based on DEM analysis of Jordan et al. (2005) and ~ 20 km dextral offset of lower Miocene sediments in the Botsara syncline, Van Hinsbergen et al. (2006) suggested Thesprotiko fault zone in western Greece, to be linking the strike-slip deformation of the KTF to the North Anatolian Fault via the transtensional Aliakmon fault. The strike of Thesprotiko fault zone seems compatible with the KTF, but its continuation into the Aliakmon fault places this tectonic boundary too much north of the KTF.

6.1.3. The Gulf of Corinth and the North Aegean Trough

Distributed *syn*-rift sedimentation in the Gulf of Corinth began around ~4 Ma, although the localized deformation started after 0,6 Ma (Armijo et al., 1996; Nixon et al., 2016; Gawthorpe et al., 2018). There is an asymmetry between the southeastern and southwestern Gulf in terms of sedimentary facies, thickness, and the position of erosional surfaces (terraces) (Papanikolaou and Royden, 2007). Moretti et al. (2003) concluded that the current pattern of extension began later in the west than the east. Assuming the present-day GNSS-derived slip rates as a proxy to the geological slip-rates, Reilinger et al. (2010) estimate the inception of the activity in the Gulf of Evia to 3 ± 1 Ma, the eastern Gulf of Corinth to 2 Ma and the western gulf to 1 Ma. The Gulf of Corinth thus opened simultaneously with, or shortly after the Epirus slab disconnected from the deeper Hellenic slab.

Armijo et al. (1999) suggest that the age of westward propagation of the North Anatolian Fault into the Aegean domain is early Pliocene on the basis of an offset anticline in the Dardanelles. Yaltırak et al. (2000) and Şengör et al. (2005) dismiss this early age due to lack of field evidence for the offset marker. Instead, Yaltırak (2002) suggests that the dextral motion of the North Anatolian Fault transferred into the Aegean domain since 4 Ma, using marine reflection studies and detailed geological mapping. This synchronicity lends support to the interpretation that there is common cause with the formation of the KTF proto-STEP fault system without, however, developing into a throughgoing STEP fault system (KTF- GC-NAT-NAF).

6.2. Our scenario for the recent evolution of the western Hellenic slab

The vertical separation between the Epirus segment and the deeper Hellenic slab in our model is consistent with the inferences from other studies. Our evolutionary scenario therefore also involves lateral propagation of a horizontal slab tear.

The original STEP fault model for the KTF (Fig. 4B; Govers and Wortel, 2005) involved a free slab edge to the Hellenic slab. Royden and Papanikolaou (2011) modified the idea by suggesting that the Hellenic slab was fragmented by a vertical tear. Suckale et al. (2009) find seismological evidence for such tear. We interpret the (semi-)vertical gap in our tomographic model to result from slab fragmentation in agreement with these earlier ideas and findings.

In Section 5.5 we estimate the time it would require for the deep Hellenic slab to subduct deeper and create the vertical distance of ~50 km to the base of the imaged Epirus fragment (~4 Ma). Our interpretation is that this gap was created by (continued) slab detachment. In the previous section we noted that this timing agrees (within uncertainty limits) with the initiation time of the KTF (~4 Ma). The implication is that slab detachment and fragmentation would have occurred near-simultaneous. A similar scenario was proposed by Wortel et al. (2009), who suggest that the southwestern edge of the Calabria slab developed from fragmentation (vertical tearing) following slab break-off beneath the Kabylies. Near KTF it is however unclear whether the fragmentation developed from slab detachment, like they propose.

Our scenario combines the models associated with Figs. 4A and B. The entry of continental Adriatic lithosphere into the west Hellenic subduction zone initiated slab detachment under the Dinarides from the Oligocene onward (Wortel and Spakman, 1992; Schefer et al., 2011; Handy et al., 2015). Pliocene detachment (Fig. 10) triggered slab fragmentation, thereby isolating the (likely more buoyant) Epirus fragment from the Hellenic slab. The critical component for the development of the proto-STEP fault may have been the redistribution of the gravitational pull, which caused the Epirus fragment to stall, and the Hellenic slab to roll back faster. This would have resulted in a significant subduction velocity difference between the two segments since the late Miocene. Direct observational constraints on this contrast in subduction rates are lacking, but in this rollback context they can be proxied by extension in the overriding plate. Papanikolaou and Royden (2007) document the change in the strikes of the normal faults from NW-SE to E-W during the late-Miocene to Pliocene. Brun et al. (2016) documented a Pliocene change in the direction of stretching from NE-SW to N-S in the Southern Hellenides, and an increase in the spreading rates. Meijer and Wortel (1996, 1997) discuss how tensile stress rotations can be understood as a response to slab-detachment below the Dinarides and western Greece. This supports our interpretation of a velocity contrast between detached and attached segments. Important was that the velocity contrast between the slab fragments persisted a few Myr, long enough to initiate the proto-STEP fault in the overriding plate. North-south extension in central Greece commenced synchronously with the isolation of the Epirus fragment from the Hellenic slab.

7. Under what conditions does a STEP evolve from slab fragmentation?

Wortel et al. (2009) were the first to consider STEP fault initiation. These authors considered relatively simple cases of STEP fault initiation, where horizontal slab breakoff developed relatively directly into vertical tears, slab edges and STEP faults. They discuss the plate boundary reorganization that began around 20 Ma and eventually resulted in the lateral northern edge of the Tonga-Kermadec slab, and the STEP fault along the north boundary of the Lau Basin. In the Mediterranean context they discuss how Miocene slab breakoff beneath the Maghrebides (northern Africa) may have evolved into the lateral edge along the south end of the Calabria slab, and the STEP fault zone in northern Sicily and in the west of the Ionian basin.

An important further insight came from Van Benthem et al. (2013), who pointed out that the long-lived slab edge beneath Hispaniola (northern Caribbean) had not developed into a STEP fault in the overriding plate. Here, the relative motion is mostly transpressive with only a small trench-perpendicular motion. The cause of this low trench-perpendicular motion is unclear but it may have to do with high resistance to (STEP) tearing of the subducting oceanic North America plate. Another cause may be that subduction of the buoyant crust of the Bahamas platform resulted in a substantial decrease of the slab pull force. Whichever the cause, it is clear that the fragmented slab needs to have a different convergence velocity than the (slab or surface plate) on the other side of the slab edge to develop a STEP fault. In a similar fashion, the absence of STEP faulting in the Dinarides margin during the Late Miocene was connected to the predominantly dextral relative motion of Adria and Moesia, where the low convergence velocity may have been a response to subduction of continental crust (e.g., van Hinsbergen et al., 2019).

Another step was taken by Govers and Fichtner (2016), following up on the work of Bartol and Govers (2014), on the uplift of Anatolia. These authors argue that slab fragmentation below west Anatolia resulted in differential roll-back between the Hellenic and Cyprus-Bitlis fragments. No well-defined STEP fault zone seems to have developed within western Anatolia during this period (35–16 Ma). Govers and Fichtner (2016) argue low mechanical coupling of the slab fragments to the overriding Anatolian surface plate. Only after the Cyprus slab rolled

back from beneath the Anatolian crust did the modern Pliny-Strabo STEP fault develop (Özbakır et al., 2013). The mechanical coupling of the slab fragments to the overriding thus likely plays a significant role in the development of a STEP fault.

Van Benthem et al. (2013) propose that the long-lived STEP fault zone that constitutes the plate boundary between the South America and Caribbean plates may have initiated ~45 Ma due to the entry of North Andes continental fragment into the Greater Antilles Subduction. They suggest that the STEP fault activity initiated along a pre-existing weak zone or material boundary that was inherited from the Paleocene collision. Pre-existing weakness zones or contrasts may thus facilitate the development and localization of a STEP fault. Their suggestion aligns with our inference that the North Aegean Trough and the Gulf of Corinth may have helped localizing the strain in the proto STEP fault (KTF zone).

The contrast in the subduction velocity, the amount of time over which it persists, mechanical coupling to, and the deformability of the overriding plate play a role in the initiation of a STEP fault once a slab is fragmented. These inferences should help us understand better why STEP faults did not develop above the fragmented slabs that we listed in Fig. 1, with the idea that some of these conditions are not met here.

A lateral slab edge was identified beneath Hispaniola by Van Benthem et al. (2013) along the North America - Caribbean plate boundary zone. The local relative motion direction is approximately parallel to the plate boundary, and the subduction velocity is small. The absence of a STEP fault in Hispaniola thus agrees with the above conditions for its initiation.

Two distinct discontinuities have been identified within the Nazca slab; beneath, Carnegie Ridge in the north (Gutscher et al., 1999) and Mocha Fracture Zone (Pesicek et al., 2012). Within the overriding plate near Carnegie Ridge, there is some indication of convergence velocity differences across the Carnegie ridge, parallel to the proposed tear. Furthermore, the dextral Dolores-Guayaquil shear zone deforms the upper plate (Gutscher et al., 1999), which might be a STEP fault candidate. Beneath the Mocha Fracture Zone, tomographic evidence (Pesicek et al., 2012) confirms a free slab edge. The dip angle of the slab segments does not change in the tomographic model (Pesicek et al., 2012). There are no observations to document contrasts in the subduction velocity of the slab segments. There also are no observations that would suggest the existence of a STEP fault in the overriding plate.

Miller et al. (2004, 2005, 2006a) presented tomographic evidence for the Izu-Bonin slab of a deep lateral tear or hole at the transition to the N Mariana slab. There are no observational constraints indicating a subduction velocity contrast between slab segments or any transcurrent faulting on the overriding oceanic Philippine slab. For the southern end of the Mariana slab, Gvirtzman and Stern (2004) suggested a N-S trending vertical tear based on slab dip changes. Observational constraints on a subduction velocity contrast of the slab segments are lacking. Fryer et al. (2003) suggested N-striking sinistral faults on the overriding Philippine Sea plate west of Guam, which might be interpreted as a STEP fault zone.

Lin et al. (2007, 2013) tomographic find evidence for vertical tearing of the Philippine Sea slab along a N-S strike near Taiwan. The relative motion between the Philippine and Eurasian plates is perpendicular to the proposed tear, which may explain the absence of observations of a STEP fault along the western edge of Okinawa backarc basin.

Further to the north Spakman and Hall (2010) identified horizontal slab detachment. The leading edge of the tear would currently be located beneath the Seram trench. However the tomographic model does not allow the identification of Seram slab fragments.

In the eastern termination of the Makran subduction zone, the tomographic model of Bijwaard and Spakman (2000) show a marked rectangular low velocity zone at 60 km depth. Earthquakes with hypocentral depths indicate pure down-dip and strike-slip focal mechanisms (Dziewonski et al., 1981; Ekström et al., 2012) supporting the STEP hypothesis. At the northern edge of the fault (Becker and Faccenna, 2011) demonstrate a strong positive residual topography that may be related to the vertical motions due to the propagating STEP. Furthermore, the surface projection of the anomalous region corresponds to the Chaman fault, which shows a gradient in the horizontal velocity field - that may be interpreted as the STEP-fault.

Available information regarding the correlations of slab edges and vertical slab tears with STEP faults in overriding plates globally is too scarce to rigorously verify the conditions for STEP fault formation that we formulated on the basis of our inferences for the KTF. The conditions appear to agree with the absence of a STEP fault in Hispaniola.

8. Conclusions

The western end of the Hellenic slab is fragmented near the Kefalonia Transform Fault. The separate Epirus fragment is roughly vertical below the southern Albanides. The Epirus fragment is laterally separated from the Hellenic slab by a low velocity zone ("gap") that we interpret as a tear. Below 150 km depth, the Epirus fragment is separated by ~50 km from the deeper Hellenic slab by a semi-horizontal gap. We estimate that the Epirus fragment disconnected from the Hellenic slab around 4 Ma, at about the time of opening of the Gulf of Corinth.

The Kefalonia Transform Fault zone, formed by the dextral Kefalonia and Lefkada faults, accommodates strike-slip within the overriding plate. We interpret the Kefalonia Transform Fault zone as a proto-STEP fault that initiated simultaneous with Pliocene fragmentation of the Epirus fragment.

In the NW part of the Ionian basin we image a sharp transition to low-velocity anomalies that aligns with the strike of the KTF. The location of the transition coincides with a gradient in free-air anomalies.

A contrast in the subduction velocity, the amount of time over which it persists, mechanical coupling to, and the deformability of, the overriding plate play a role in the initiation of a STEP fault once a slab is fragmented. Particularly the absence of a contrast in the subduction velocity of slab fragments prevents the development of STEP faults above currently fragmented slabs.

These constraints likely determined the development of the KTF proto STEP fault, and the development, or not, of other STEP faults worldwide.

Supplementary data to this article can be found online at https://doi.org/10.1016/j.tecto.2020.228471.

Declaration of competing interest

The authors declare that they have no known competing financial interests or personal relationships that could have appeared to influence the work reported in this paper.

Acknowledgements

Careful reviews by Stefan Schmid and an anonymous reviewer were very valuable in helping us focus and create a much improved manuscript. We also thank the editor-in-chief, Philippe Agard, for his guidance. Figures are created using GMT software (Wessel and Smith, 1998). ADO was funded by the Netherlands Research Center for Integrated Solid Earth Science (ISES) at Utrecht University.

References

Agard, P., Omrani, J., Jolivet, L., Whitechurch, H., Vrielynck, B., Spakman, W., Monie, P., Meyer, B., Wortel, R., 2011. Zagros orogeny: a subduction-dominated process. Geol. Mag. 148, 692–725.

Armijo, R., Meyer, B., King, G.C.P., Rigo, A., Papanastassiou, D., 1996. Quaternary evolution of the Corinth Rift and its implications for the Late Cenozoic evolution of the Aegean. Geophys. J. Int. 126, 11–53.

Armijo, R., Meyer, B., Hubert, A., Barka, A., 1999. Westward propagation of the North

Anatolian fault into the northern Aegean: timing and kinematics. Geology 27, 267–270. https://doi.org/10.1130/0091-7613(1999)027<0267:WPOTNA>2.3.CO;2.
Babuska, V., Cara, M., 1991. Seismic Anisotropy in the Earth. Vol. 10 Springer Science & Business Media.
Baes, M., Govers, R., Wortel, M.J.R., 2011. Subduction initiation along the inherited weakness zone at the edge of a slab: insights from numerical models. Geophys. J. Int. 184, 991–1008.
Baker, C., Hatzfeld, D., Lyon-Caen, H., Papadimitriou, E., Rigo, A., 1997. Earthquake mechanisms of the Adriatic Sea and Western Greece: implications for the oceanic subduction-continental collision transition. Geophys. J. Int. 131, 559–594.
Bartol, J., Govers, R., 2014. A single cause for uplift of the Central and Eastern Anatolian plateau? Tectonophysics 637, 116–136.
Basili, R., Kastelic, V., Demircioglu, M., Garcia Moreno, D., Nemser, E., Petricca, P., Sboras, S., Besana Ostman, G., Cabral, J., Camelbeeck, T., Caputo, R., Danciu, L., Domac, H., Fonseca, J., García-Mayordomo, J., Giardini, D., Glavatovic, B., Gulen, L., Ince, Y., Pavlides, S., Sesetyan, K., Tarabusi, G., Tiberti, M., Utkucu, M., Valensise, G., Vanneste, K., Vilanova, S., Wössner, J., 2013. The European Database of Seismogenic Faults (EDSF) Compiled in the Framework of the Project SHARE. URL. http://diss.rm.ingv.it/share-edsf/https://doi.org/10.6092/INGV.IT-SHARE-EDSF.
Bastow, I.D., 2012. Relative arrival-time upper-mantle tomography and the elusive background mean. Geophys. J. Int. 190, 1271–1278.
Becker, T., Faccenna, C., 2011. Mantle conveyor beneath the Tethyan collisional belt. Earth Planet. Sci. Lett. 310, 453–461.
Bega, Z., 2015. Hydrocarbon exploration potential of Montenegro–a brief review. J. Pet. Geol. 38, 317–330.
Biermanns, P., Schmitz, B., Ustaszewski, K., Reicherter, K., 2019. Tectonic geomorphology and Quaternary landscape development in the Albania-Montenegro border region: an inventory. Geomorphology 326, 116–131.
Bijwaard, H., Spakman, W., 2000. Non-linear global P-wave tomography by iterated linearized inversion. Geophys. J. Int. 141, 71–82.
Bijwaard, H., Spakman, W., Engdahl, E., 1998. Closing the gap between regional and global travel time tomography. J. Geophys. Res. 103, 30055–30078.
Bird, P., 2003. An updated digital model of plate boundaries. Geochem. Geophys. Geosyst. 4, 1027. https://doi.org/10.1029/2001GC000252.
Biryol, C., Beck, S., Zandt, G., Özacar, A., 2011. Segmented African lithosphere beneath the Anatolian region inferred from teleseismic P-wave tomography. Geophys. J. Int. 1, 16.
Bocchini, G., Brüstle, A., Becker, D., Meier, T., van Keken, P., Ruscic, M., Papadopoulos, G., Rische, M., Friederich, W., 2018. Tearing, segmentation, and backstepping of subduction in the Aegean: new insights from seismicity. Tectonophysics 734, 96–118.
Bourova, E., Kassaras, I., Pedersen, H.A., Yanovskaya, T., Hatzfeld, D., Kiratzi, A., 2005. Constraints on absolute S velocities beneath the Aegean Sea from surface wave analysis. Geophys. J. Int. 160, 1006–1019.
Brun, J.P., Faccenna, C., Gueydan, F., Sokoutis, D., Philippon, M., Kydonakis, K., Gorini, C., 2016. The two-stage Aegean extension, from localized to distributed, a result of slab rollback acceleration. Can. J. Earth Sci. 53, 1142–1157.
Burchfiel, B.C., King, R.W., Todosov, A., Kotzev, V., Durmurdzanov, N., Serafimovski, T., Nurce, B., 2006. GPS results for Macedonia and its importance for the tectonics of the Southern Balkan extensional regime. Tectonophysics 413, 239–248.
Burgos, G., Montagner, J.P., Beucler, E., Capdeville, Y., Mocquet, A., Drilleau, M., 2014. Oceanic lithosphere-asthenosphere boundary from surface wave dispersion data. J. Geophys. Res. 119, 1079–1093.
Carminati, E., Wortel, M.J.R., Meijer, P., Sabadini, R., 1998. The two-stage opening of the western-central Mediterranean basins: a forward modeling test to a new evolutionary model. Earth Planet. Sci. Lett. 160, 667–679.
Chamot-Rooke, N., Rangin, C., Le Pichon, X., Dotmed working group, 2005. DOTMED (Deep Offshore Tectonics of the Mediterranean): A Synthesis of deep marine data in the Eastern Mediterranean. Mémoires de la Société Géologique de France 177.
Chousianitis, K., Ganas, A., Evangelidis, C.P., 2015. Strain and rotation rate patterns of mainland Greece from continuous GPS data and comparison between seismic and geodetic moment release. J. Geophys. Res. 120, 3909–3931.
Clark, S., Sobiesiak, M., Zelt, C., Magnani, M., Miller, M., Bezada, M., Levander, A., 2008. Identification and tectonic implications of a tear in the South American plate at the southern end of the Lesser Antilles. Geochem. Geophys. Geosyst. 9.
Clews, J.E., 1989. Structural controls on basin evolution: neogene to quaternary of the Ionian zone, Western Greece. J. Geol. Soc. 146, 447–457.
Copley, A., Boait, F., Hollingsworth, J., Jackson, J., McKenzie, D., 2009. Subparallel thrust and normal faulting in Albania and the roles of gravitational potential energy and rheology contrasts in mountain belts. J. Geophys. Res. 114 (B5).
Crotwell, H.P., Owens, T.J., Ritsema, J., 1999. The taup toolkit: flexible seismic travel-time and ray-path utilities. Seismol. Res. Lett. 70, 154–160.
D'Agostino, N., Avallone, A., Cheloni, D., D' Anastasio, E., Mantenuto, S., Selvaggi, G., 2008. Active tectonics of the Adriatic region from GPS and earthquake slip vectors. J. Geophys. Res. 113.
de Lis Mancilla, F., Heit, B., Morales, J., Yuan, X., Stich, D., Molina-Aguilera, A., Azañon, J., Martín, R., 2018. A step fault in central betics, associated with lateral lithospheric tearing at the northern edge of the Gibraltar arc subduction system. Earth Planet. Sci. Lett. 486, 32–40.
Duermeijer, C., Krijgsman, W., Langereis, C., Meulenkamp, J., Triantaphyllou, M., Zachariasse, W., 1999. A late Pleistocene clockwise rotation phase of Zakynthos (Greece) and implications for the evolution of the western Aegean arc. Earth Planet. Sci. Lett. 173, 315–331.
Duermeijer, C., Nyst, M., Meijer, P., Langereis, C., Spakman, W., 2000. Neogene evolution of the Aegean arc: paleomagnetic and geodetic evidence for a rapid and young rotation phase. Earth Planet. Sci. Lett. 176, 509–526.
Dziewonski, A.M., Chou, T.A., Woodhouse, J.H., 1981. Determination of earthquake source parameters from waveform data for studies of global and regional seismicity. J. Geophys. Res. 86, 2825–2852.
Ekström, G., Nettles, M., Dziewonski, A.M., 2012. The global CMT project 2004–2010: centroid-moment tensors for 13,017 earthquakes. Phys. Earth Planet. Inter. 200-201, 1–9.
Evangelidis, C.P., 2017. Seismic anisotropy in the Hellenic subduction zone: effects of slab segmentation and subslab mantle flow. Earth Planet. Sci. Lett. 480, 97–106.
Faccenna, C., Becker, T., Miller, M., Serpelloni, E., Willett, S., 2014. Isostasy, dynamic topography, and the elevation of the Apennines of Italy. Earth Planet. Sci. Lett. 407, 163–174.
Fichtner, A., Trampert, J., Cupillard, P., Saygin, E., Taymaz, T., Capdeville, Y., Villasenor, A., 2013. Multiscale full waveform inversion. Geophys. J. Int. 194, 534–556.
Forsyth, D., 1975. Fault plane solutions and tectonics of the South Atlantic and Scotia Sea. J. Geophys. Res. 80, 1429–1443.
Fruehn, J., Reston, T., von Huene, R., Bialas, J., 2002. Structure of the Mediterranean Ridge accretionary complex from seismic velocity information. Mar. Geol. 186, 43–58.
Fryer, P., Becker, N., Appelgate, B., Martinez, F., Edwards, M., Fryer, G., 2003. Why is the challenger deep so deep? Earth Planet. Sci. Lett. 211, 259–269.
Ganas, A., Parsons, T., 2009. Three-dimensional model of Hellenic Arc deformation and origin of the Cretan uplift. J. Geophys. Res. 114, B06404. https://doi.org/10.1029/2008JB005599.
Gawthorpe, R., Leeder, M., Kranis, H., Skourtsos, E., Andrews, J., Henstra, G., Mack, G., Muravchik, M., Turner, J., Stamatakis, M., 2018. Tectono-sedimentary evolution of the Plio-Pleistocene Corinth rift, Greece. Basin Res. 30, 448–479.
Giardini, D., Wössner, J., Danciu, L., 2014. Mapping Europe's seismic hazard. EOS Trans. Am. Geophys. Union 95, 261–262.
Gong, W., Xing, J., Jiang, X., 2018. Heterogeneous subduction structure within the Pacific plate beneath the Izu-Bonin arc. J. Geodyn. 116, 1–12.
Govers, R., Fichtner, A., 2016. Signature of slab fragmentation beneath Anatolia from full-waveform tomography. Earth Planet. Sci. Lett. 450, 10–19.
Govers, R., Wortel, M., 2005. Lithosphere tearing at STEP faults: response to edges of subduction zones. Earth Planet. Sci. Lett. 236, 505–523. https://doi.org/10.1016/j.epsl.2005.03.022.
Gutscher, M., Malavieille, J., Lallemand, S., Collot, J., 1999. Tectonic segmentation of the North Andean margin: impact of the Carnegie Ridge collision. Earth Planet. Sci. Lett. 168, 255–270.
Gvirtzman, Z., Stern, R., 2004. Bathymetry of Mariana trench-arc system and formation of the challenger deep as a consequence of weak plate coupling. Tectonics 23, TC2011.
Halpaap, F., Rondenay, S., Ottemöller, L., 2018. Seismicity, deformation, and metamorphism in the Western Hellenic Subduction Zone: new constraints from tomography. J. Geophys. Res. 123, 3000–3026.
Handy, M., Ustaszewski, K., Kissling, E., 2015. Reconstructing the Alps–Carpathians–Dinarides as a key to understanding switches in subduction polarity, slab gaps and surface motion. Int. J. Earth Sci. 104, 1–26.
Handy, M.R., Giese, J., Schmid, S.M., Pleuger, J., Spakman, W., Onuzi, K., Ustaszewski, K., 2019. Coupled crust-mantle response to slab tearing, bending, and rollback along the Dinaride-Hellenide orogen. Tectonics 38, 2803–2828.
Hansen, S., Evangelidis, C., Papadopoulos, G., 2019. Imaging slab detachment within the Western Hellenic Subduction Zone. Geochem. Geophys. Geosyst. 20, 895–912.
Hayes, G., Moore, G., Portner, D., Hearne, M., Flamme, H., Furtney, M., Smoczyk, G., 2018. Slab2, a comprehensive subduction zone geometry model. Science 362, 58–61.
Hirn, A., Sachpazi, M., Siliqi, R., Mc Bride, J., Marnelis, F., Cernobori, L., STREAMERS - PROFILES, 1996. A traverse of the Ionian islands front with coincident normal incidence and wide-angle seismics. Tectonophysics 264, 35–49.
Isacks, B., Sykes, L., Oliver, J., 1969. Focal mechanisms of deep and shallow earthquakes in the Tonga-Kermadec region and the tectonics of Island Arcs. Geol. Soc. Am. Bull. 80, 1443–1470.
Jolivet, L., Faccenna, C., Huet, B., Labrousse, L., Le Pourhiet, L., Lacombe, O., Lecomte, E., Burov, E., Denèle, Y., Brun, J.P., Philippon, M., Paul, A., Salaün, G., Karabulut, H., Piromallo, C., Monié, P., Gueydan, F., Okay, A., Oberhänsli, R., Pourteau, A., Augier, R., Gadenne, L., Driussi, O., 2013. Aegean tectonics: strain localisation, slab tearing and trench retreat. Tectonophysics 597, 1–33.
Jordan, G., Meijninger, B., Van Hinsbergen, D., Meulenkamp, J., Van Dijk, P., 2005. Extraction of morphotectonic features from DEMs: development and applications for study areas in Hungary and NW Greece. Int. J. Appl. Earth Obs. Geoinf. 7, 163–182.
Jouanne, F., Mugnier, J.L., Koci, R., Bushati, S., Matev, K., Kuka, N., Shinko, I., Kociu, S., Duni, L., 2012. GPS constraints on current tectonics of Albania. Tectonophysics 554, 50–62.
Karabulut, H., Paul, A., Özbakır, A., Ergün, T., Şentürk, S., 2019. A new crustal model of the Anatolia-Aegean domain: evidence for the dominant role of isostasy in the support of the Anatolian plateau. Geophys. J. Int. 218, 57–73.
Kassaras, I., Kapetanidis, V., Karakonstantis, A., 2016. On the spatial distribution of seismicity and the 3D tectonic stress field in western Greece. Phys. Chem. Earth A/B/C 95, 50–72.
Kaviris, G., Fountoulakis, I., Spingos, I., Millas, C., Papadimitriou, P., Drakatos, G., 2018. Mantle dynamics beneath Greece from SKS and PKS seismic anisotropy study. Acta Geophys. 66, 1341–1357.
Kennett, B., Engdahl, E., Buland, R., 1995. Constraints on seismic velocities in the earth from traveltimes. Geophys. J. Int. 122, 108–124.
Kiratzi, A., Benetatos, C., 2008. The 6 January 2008 (Mw6.2) Leonidio (Southern Greece) Intermediate Depth Earthquake: Teleseismic Body Wave Modelling. Technical Report. EMSC.
Kiratzi, A., Louvari, E., 2003. Focal mechanisms of shallow earthquakes in the Aegean Sea and the surrounding lands determined by waveform modelling: a new database. J.

Geodyn. 36, 251–274.
Kissel, C., Speranza, F., Milicevic, V., 1995. Paleomagnetism of external southern and central Dinarides and northern Albanides: implications for the Cenozoic activity of the Scutari-Pec Transverse Zone. J. Geophys. Res. 100, 14999–15007.
Korbar, T., 2009. Orogenic evolution of the external Dinarides in the NE Adriatic region: a model constrained by tectonostratigraphy of Upper Cretaceous to Paleogene carbonates. Earth-Sci. Rev. 96, 296–312.
Kotzev, V., Nakov, R., Georgiev, T., Burchfiel, B.C., King, R.W., 2006. Crustal motion and strain accumulation in western Bulgaria. Tectonophysics 413, 127–145. https://doi.org/10.1016/j.tecto.2005.10.040.
Koulakov, I., Kaban, M., Tesauro, M., Cloetingh, S., 2009. P-and S-velocity anomalies in the upper mantle beneath Europe from tomographic inversion of ISC data. Geophys. J. Int. 179, 345–366.
Kreemer, C., Chamot-Rooke, N., Le Pichon, X., 2004. Constraints on the evolution and vertical coherency of deformation in the Northern Aegean from a comparison of geodetic, geologic and seismologic data. Earth Planet. Sci. Lett. 225, 329–346.
Kumar, P., Srijayanthi, G., Ravi Kumar, M., 2016. Seismic evidence for tearing in the subducting indian slab beneath the andaman arc. Geophys. Res. Lett. 43, 4899–4904.
Lallemand, S., Liu, C., Font, Y., 1997. A tear fault boundary between the Taiwan orogen and the Ryukyu subduction zone. Tectonophysics 274, 171–190.
Laske, G., Masters, G., Ma, Z., Pasyanos, M., 2013. Update on CRUST1. 0—A 1-degree global model of Earth's crust. In: Geophysical Research Abstracts 15, 2658. EGU General Assembly, Vienna, Austria.
Lay, T., Wallace, T.C., 1995. Modern Global Seismology. Academic Press.
Le Breton, E., Handy, M., Molli, G., Ustaszewski, K., 2017. Post-20 Ma motion of the Adriatic plate – new constraints from surrounding orogens and implications for crust-mantle decoupling. Tectonics 36, 3135–3154.
Le Pichon, X., 1982. Land-locked oceanic basins and continental collision: the Eastern Mediterranean as a case example. In: Hsu, K.J. (Ed.), Symposium of Mountain Building. Academic Press, London, pp. 201–211.
Lentas, K., Di Giacomo, D., Harris, J., Storchak, D.A., 2019. The ISC Bulletin as a comprehensive source of earthquake source mechanisms. Earth Syst. Sci. Data 11, 565–578.
Lin, J.Y., Sibuet, J.C., Lee, C.S., Hsu, S.K., Klingelhoefer, F., 2007. Origin of the southern Okinawa Trough volcanism from detailed seismic tomography. J. Geophys. Res. 112, B08308.
Lin, J., Hsu, S., Sibuet, J., Lee, C., Liang, C., 2013. Plate tearing in the northwestern corner of the subducting Philippine Sea Plate. J. Asian Earth Sci. 70, 1–7.
Louvari, E., Kiratzi, A., Papazachos, B., 1999. The Cephalonia transform fault and its extension to western Lefkada island (Greece). Tectonophysics 308, 223–236.
McClusky, S., Balassanian, S., Barka, A., Demir, C., Ergintav, S., Georgiev, I., Gurkan, O., Hamburger, M., Hurst, K., Kahle, H., Kastens, K., Kekelidze, G., King, R., Kotzev, V., Lenk, O., Mahmoud, S., Mistin, A., Nadariya, M., Ouzounis, A., Paradissis, D., Peter, Y., Prilepin, M., Reilinger, R., Sanli, I., Seeger, H., Tealeb, A., Toksoz, M., Veis, G., 2000. Global positioning system constraints on plate kinematics and dynamics in the eastern Mediterranean and Caucasus. J. Geophys. Res. 105, 5695–5719.
Meijer, P.T., Wortel, M.J.R., 1996. Temporal variation in the stress field of the Aegean region. Geophys. Res. Lett. 23, 439–442.
Meijer, P.T., Wortel, M.J.R., 1997. Present-day dynamics of the Aegean region: a model analysis of the horizontal pattern of stress and deformation. Tectonics 16, 879–895.
Metois, M., D' Agostino, N., Avallone, A., Chamot-Rooke, N., Rabaute, A., Duni, L., Kuka, N., Koci, R., Georgiev, I., 2015. Insights on continental collisional processes from GPS data: dynamics of the peri-Adriatic belts. J. Geophys. Res. 120, 8701–8719.
Millen, D., Hamburger, M., 1998. Seismological evidence for tearing of the Pacific plate at the northern termination of the Tonga subduction zone. Geology 26, 659–662.
Miller, M., Piana-Agostinetti, N., 2011. Erosion of the continental lithosphere at the cusps of the Calabrian arc: evidence from S receiver functions analysis. Geophys. Res. Lett. 38.
Miller, M., Kennett, B., Lister, G., 2004. Imaging changes in morphology, geometry, and physical properties of the subducting Pacific plate along the Izu–Bonin–Mariana arc. Earth Planet. Sci. Lett. 224, 363–370.
Miller, M., Gorbatov, A., Kennett, B., 2005. Heterogeneity within the subducting Pacific slab beneath the Izu–Bonin–Mariana arc: evidence from tomography using 3D ray tracing inversion techniques. Earth Planet. Sci. Lett. 235, 331–342.
Miller, M., Gorbatov, A., Kennett, B., 2006a. Three-dimensional visualization of a near-vertical slab tear beneath the southern Mariana arc. Geochem. Geophys. Geosyst. 7.
Miller, M., Kennett, B., Toy, V., 2006b. Spatial and temporal evolution of the subducting Pacific plate structure along the western Pacific margin. J. Geophys. Res. Solid Earth 111.
Moretti, I., Sakellariou, D., Lykousis, V., Micarelli, L., 2003. The Gulf of Corinth: an active half graben? J. Geodyn. 36, 323–340.
Neely, J.S., Furlong, K.P., 2018. Evidence of displacement-driven maturation along the San Cristobal Trough transform plate boundary. Earth Planet. Sci. Lett. 485, 88–98.
Nixon, C.W., McNeill, L., Bull, J., Bell, R., Gawthorpe, R., Henstock, T., Christodoulou, D., Ford, M., Taylor, B., Sakellariou, D., Ferentinos, G., Collier, R., Goodliffe, A., Sachpazi, M., Kranis, H., 2016. Rapid spatiotemporal variations in rift structure during development of the Corinth Rift, Central Greece. Tectonics 35, 1225–1248.
Nocquet, J., 2012. Present-day kinematics of the Mediterranean: a comprehensive overview of GPS results. Tectonophysics 579, 220–242.
Özbakır, A.D., Şengör, A., Wortel, M., Govers, R., 2013. The Pliny–Strabo trench region: a large shear zone resulting from slab tearing. Earth Planet. Sci. Lett. 375, 188–195.
Papanikolaou, D.J., Royden, L.H., 2007. Disruption of the Hellenic arc: Late Miocene extensional detachment faults and steep Pliocene-Quaternary normal faults—Or what happened at Corinth? Tectonics 26.
Papanikolaou, D., Fountoulis, I., Metaxas, C., 2007. Active faults, deformation rates and Quaternary paleogeography at Kyparissiakos Gulf (SW Greece) deduced from onshore and offshore data. Quat. Int. 171, 14–30.
Papazachos, C., Nolet, G., 1997. P and S deep velocity structure of the Hellenic area obtained by robust nonlinear inversion of travel times. J. Geophys. Res. Solid Earth 102, 8349–8367.
Papazachos, B., Karakostas, V., Papazachos, C., Scordilis, E., 2000. The geometry of Wadati-Benioff zone and lithospheric kinematics of the Hellenic arc. Tectonophysics 319, 275–300. https://doi.org/10.1016/S0040-1951(99)00299-1.
Pearce, F., Rondenay, S., Sachpazi, M., Charalampakis, M., Royden, L., 2012. Seismic investigation of the transition from continental to oceanic subduction along the western Hellenic Subduction Zone. J. Geophys. Res. Solid Earth 117.
Perouse, E., Chamot-Rooke, N., Rabaute, A., Briole, P., Jouanne, F., Georgiev, I., Dimitrov, D., 2012. Bridging onshore and offshore present-day kinematics of central and eastern Mediterranean: implications for crustal dynamics and mantle flow. Geochem. Geophys. Geosyst. 13.
Pesicek, J., Engdahl, E., Thurber, C., DeShon, H., Lange, D., 2012. Mantle subducting slab structure in the region of the 2010 M 8.8 Maule earthquake (30–40 S), Chile. Geophys. J. Int. 191, 317–324.
Piromallo, C., Morelli, A., 2003. P wave tomography of the mantle under the Alpine-Mediterranean area. J. Geophys. Res. 108, 2065. https://doi.org/10.1029/2002JB001757.
Pondrelli, S., Salimbeni, S., Ekström, G., Morelli, A., Gasperini, P., Vannucci, G., 2006. The Italian CMT dataset from 1977 to the present. Phys. Earth Planet. Inter. 159, 286–303.
Pondrelli, S., Salimbeni, S., Morelli, A., Ekström, G., Boschi, E., 2007. European-mediterranean regional centroid moment tensor catalog: solutions for years 2003 and 2004. Phys. Earth Planet. Inter. 164, 90–112.
Pondrelli, S., Salimbeni, S., Morelli, A., Ekstrom, G., Postpischl, L., Vannucci, G., Boschi, E., 2011. European-mediterranean regional centroid moment tensor catalog: solutions for 2005–2008. Phys. Earth Planet. Inter. 185, 74–81.
Reilinger, R., McClusky, S., Paradissis, D., Ergintav, S., Vernant, P., 2010. Geodetic constrains on the tectonic evolution of the Aegean region and strain accumulation along Hellenic subduction zone. Tectonophysics 488, 22–30. https://doi.org/10.1016/j.tecto.2009.05.027.
Reyners, M., Robertson, E.J., 2004. Intermediate depth earthquakes beneath nelson, new zealand, and the southwestern termination of the subducted pacific plate. Geophys. Res. Lett. 31.
Royden, L., 1993. Evolution of retreating subduction boundaries formed during continental collision. Tectonics 12, 629–638.
Royden, L., Papanikolaou, D., 2011. Slab segmentation and Late Cenozoic disruption of the Hellenic arc. Geochem. Geophys. Geosyst. 12, Q03010.
Russo, R., Speed, R., Okal, E., Shepherd, J., Rowley, K., 1993. Seismicity and tectonics of the southeastern Caribbean. J. Geophys. Res. 98, 14299–14319.
Sachpazi, M., Laigle, M., Charalampakis, M., Diaz, J., Kissling, E., Gesret, A., Becel, A., Flueh, E., Miles, P., Hirn, A., 2016. Segmented Hellenic slab rollback driving Aegean deformation and seismicity. Geophys. Res. Lett. 43, 651–658.
Salaün, G., Pedersen, H.A., Paul, A., Farra, V., Karabulut, H., Hatzfeld, D., Papazachos, C., Childs, D.M., Pequegnat, C., Team, S., 2012. High-resolution surface wave tomography beneath the Aegean-Anatolia region: constraints on upper-mantle structure. Geophys. J. Int. 190, 406–420.
Schefer, S., Cvetković, V., Fügenschuh, B., Kounov, A., Ovtcharova, M., Schaltegger, U., Schmid, S., 2011. Cenozoic granitoids in the Dinarides of southern Serbia: age of intrusion, isotope geochemistry, exhumation history and significance for the geodynamic evolution of the Balkan Peninsula. Int. J. Earth Sci. 100, 1181–1206.
Şengör, A.M.C., Tüysüz, O., Imren, C., Sakınç, M., Eyidoğan, H., Görür, N., Le Pichon, X., Rangin, C., 2005. The North Anatolian Fault: a new look. Annu. Rev. Earth Planet. Sci. 33, 37–112. https://doi.org/10.1146/annurev.earth.32.101802.120415.
Shaw, B., Jackson, J., 2010. Earthquake mechanisms and active tectonics of the Hellenic subduction zone. Geophys. J. Int. 181, 966–984. https://doi.org/10.1111/j.1365-246X.2010.04551.x.
Sippl, C., Schurr, B., Yuan, X., Mechie, J., Schneider, F., Gadoev, M., Orunbaev, S., Oimahmadov, I., Haberland, C., Abdybachaev, U., et al., 2013. Geometry of the Pamir-Hindu Kush intermediate-depth earthquake zone from local seismic data. J. Geophys. Res. 118, 1438–1457.
Sobel, E.R., Chen, J., Schoenbohm, L.M., Thiede, R., Stockli, D.F., Sudo, M., Strecker, M.R., 2013. Oceanic-style subduction controls late cenozoic deformation of the northern Pamir orogen. Earth Planet. Sci. Lett. 363, 204–218.
Sodoudi, F., Kind, R., Hatzfeld, D., Priestley, K., Hanka, W., Wylegalla, K., Stavrakakis, G., Vafidis, A., Harjes, H., Bohnhoff, M., et al., 2006. Lithospheric structure of the Aegean obtained from P and S receiver functions. J. Geophys. Res. 111, B12307.
Spakman, W., Hall, R., 2010. Surface deformation and slab–mantle interaction during Banda arc subduction rollback. Nat. Geosci. 3, 562.
Spakman, W., Wortel, M.J.R., Vlaar, N.J., 1988. The Hellenic subduction zone: a tomographic image and its geodynamic implications. Geophys. Res. Lett. 15, 60–63.
Spakman, W., van der Lee, S., van der Hilst, R., 1993. Travel-time tomography of the European-Mediterranean mantle down to 1400 km. Phys. Earth Planet. Inter. 79, 3–74.
Speranza, F., Minelli, L., Pignatelli, A., Chiappini, M., 2012. The Ionian Sea: the oldest in situ ocean fragment of the world? J. Geophys. Res. 117.
Suckale, J., Rondenay, S., Sachpazi, M., Charalampakis, M., Hosa, A., Royden, L.H., 2009. High-resolution seismic imaging of the western Hellenic subduction zone using teleseismic scattered waves. Geophys. J. Int. 178, 775–791. https://doi.org/10.1111/j.1365-246X.2009.04170.x.
Sunilkumar, T., Earnest, A., Silpa, K., Andrews, R., 2019. Rupture of the indian slab in the 2011 mw 6.9 Sikkim Himalaya earthquake and its tectonic implications. J. Geophys. Res. 124, 2623–2637.
Thiede, R.C., Sobel, E.R., Chen, J., Schoenbohm, L.M., Stockli, D.F., Sudo, M., Strecker,

M.R., 2013. Late cenozoic extension and crustal doming in the India-Eurasia collision zone: new thermochronologic constraints from the NE Chinese Pamir. Tectonics 32, 763–779.
Tugend, J., Chamot-Rooke, N., Arsenikos, S., Blanpied, C., Frizon de Lamotte, D., 2019. Geology of the Ionian Basin and margins: a key to the East Mediterranean geodynamics. Tectonics 38 (8), 2668–2702. https://doi.org/10.1029/2018TC005472.
Underhill, J., 1989. Late Cenozoic deformation of the Hellenide foreland, western Greece. Geol. Soc. Am. Bull. 101, 613–634.
Van Benthem, S., Govers, R., Spakman, W., Wortel, R., 2013. Tectonic evolution and mantle structure of the Caribbean. J. Geophys. Res. Solid Earth 118, 3019–3036.
Van der Meer, D., Van Hinsbergen, D., Spakman, W., 2018. Atlas of the underworld: slab remnants in the mantle, their sinking history, and a new outlook on lower mantle viscosity. Tectonophysics 723, 309–448.
Van Hinsbergen, D.J., Schmid, S.M., 2012. Map view restoration of Aegean–West Anatolian accretion and extension since the Eocene. Tectonics 31.
Van Hinsbergen, D.J.J., Langereis, C.G., Meulenkamp, J.E., 2005. Revision of the timing, magnitude and distribution of Neogene rotations in the western Aegean region. Tectonophysics 396, 1–34. https://doi.org/10.1016/j.tecto.2004.10.001.
Van Hinsbergen, D.J.J., Van der Meer, D.G., Zachariasse, W.J., Meulenkamp, J.E., 2006. Deformation of western Greece during Neogene clockwise rotation and collision with Apulia. Int. J. Earth Sci. 95, 463–490. https://doi.org/10.1007/s00531-005-0047-5.
Van Hinsbergen, D.J.J., Torsvik, T.H., Schmid, S.M., Maţenco, L.C., Maffione, M., Vissers, R.L.M., et al., 2019. Orogenic architecture of the Mediterranean region and kinematic reconstruction of its tectonic evolution since the Triassic. Gondwana Res. 1–427. https://doi.org/10.1016/j.gr.2019.07.009.
Van Unen, M., Matenco, L., Nader, F., Dernault, R., Mandic, O., Demir, V., 2019. Kinematics of foreland-vergent crustal accretion: inferences from the Dinarides evolution. Tectonics 38, 49–76.
Vassilakis, E., Royden, L., Papanikolaou, D., 2011. Kinematic links between subduction along the Hellenic trench and extension in the Gulf of Corinth, Greece: a multidisciplinary analysis. Earth Planet. Sci. Lett. 303, 108–120.
Wessel, P., Smith, W.H.F., 1998. New, improved version of generic mapping tools released. EOS Trans. Am. Geophys. Union 79, 579.
Weston, J., Engdahl, E., Harris, J., Di Giacomo, D., Storchak, D., 2018. ISC-EHB: reconstruction of a robust earthquake data set. Geophys. J. Int. 214, 474–484.
Wortel, M.J.R., Spakman, W., 1992. Structure and dynamics of subducted lithosphere in the Mediterranean region. In: Proceedings of the Koninklijke Nederlandse Akademie van Wetenschappen, pp. 325–347.
Wortel, M.J.R., Spakman, W., 2000. Subduction and slab detachment in the Mediterranean – Carpathian region. Science 290, 1910–1917. https://doi.org/10.1126/science.290.5498.1910.
Wortel, R., Govers, R., Spakman, W., 2009. Continental collision and the STEP-wise evolution of convergent plate boundaries: from structure to dynamics. Subduction Zone Geodynamics. In: Lallemand, S., Funiciello, F. (Eds.), Subduction Zone Geodynamics. Frontiers in Earth Sciences. Springer, Berlin, Heidelberg, pp. 47–59.
Yaltırak, C., 2002. Tectonic evolution of the Marmara Sea and its surroundings. Mar. Geol. 190, 493–529.
Yaltırak, C., Sakınç, M., Oktay, F., 2000. Westward propagation of North Anatolian fault into the northern Aegean: timing and kinematics: comment and Reply. Geology 28, 187.
Zahradnik, J., Gallovic, F., Sokos, E., Serpetsidaki, A., Tselentis, A., 2008. Quick fault-plane identification by a geometrical method: application to the Mw 6.2 Leonidio earthquake, 6 January 2008. Greece. Seismol. Res. Lett. 79, 653–662.
Zhang, Y., Wang, R., Walter, T.R., Feng, W., Chen, Y., Huang, Q., 2017. Significant lateral dip changes may have limited the scale of the 2015 mw 7.8 Gorkha earthquake. Geophys. Res. Lett. 44, 8847–8856.
Zhu, H., Bozdağ, E., Tromp, J., 2015. Seismic structure of the European upper mantle based on adjoint tomography. Geophys. J. Int. 201, 18–52.